



Università  
di Catania

International PhD Program in Neuroscience

XXXV cycle

PhD Coordinator: Prof. Claudio Bucolo

Doctoral Dissertation

***“Clobetasol- induced neuromuscular plasticity and neuroglial axis  
modulation in an experimental model of selective motoneurons  
depletion”***

PhD Candidate:

Federica Maria Spitale

University of Catania, Catania (Italy)

Department of Biomedical and Biotechnological Sciences

Section of Physiology

Supervisors:

Prof. Rosalba Parenti

Prof. Giovanni Li Volti

Prof. Nunzio Vicario

*To my family*

*“As long as our brain is a mystery,  
the universe,  
the reflection of the structure of the brain,  
will also be a mystery.”*

*Santiago Ramón y Cajal*

I, the undersigned Federica Maria Spitale,

Place of Birth: Catania (IT)

Date of Birth: 2<sup>nd</sup> December 1994

Author of the PhD thesis entitled:

*“Clobetasol- induced neuromuscular plasticity and neuroglial axis modulation in an experimental model of selective motoneurons depletion”*

It is not allowed to copy or to reproduce, in whole or in part, the data and the contents of the thesis.

The whole project or part of it have already been submitted to a publisher or are in press.

La sottoscritta Federica Maria Spitale,

Nata a: Catania (IT)

Data di nascita: 2 Dicembre 1994

Autrice della tesi dal titolo:

*“Plasticità neuromuscolare clobetasol mediata e modulazione dell’asse neurogliale in un modello sperimentale di deplezione selettiva dei motoneuroni”*

É fatto divieto di copiare o di riprodurre, in tutto o in parte, i dati ed i contenuti della tesi.

L’intera ricerca o parti di essa sono state già sottoposte a un editore o sono in attesa di pubblicazione.

Catania,

13 September 2022 / 13 Settembre 2022

Federica Maria Spitale



## **TABLE OF CONTENTS**

<b>SUMMARY</b>	<i>p.7</i>
<b>INTRODUCTION</b>	<i>p.9</i>
<i>Definition and clinical features of amyotrophic lateral sclerosis (ALS)</i>	<i>p.9</i>
<i>Epidemiology and etiology of ALS</i>	<i>p.10</i>
<i>Pathophysiology of ALS</i>	<i>p.11</i>
<i>Diagnostic and therapeutic approaches</i>	<i>p.13</i>
<i>Sonic hedgehog signaling pathway</i>	<i>p.15</i>
<i>Experimental animal model of selective motoneurons depletion:     CTB-Sap model</i>	<i>p.16</i>
<b>AIMS OF THIS THESIS</b>	<i>p.17</i>
<b>RESULTS</b>	<i>p.18</i>
<i>Increased expression of connexin 43 in a mouse model of spinal     motoneuronal loss</i>	<i>p.19</i>
<i>Clobetasol promotes neuromuscular plasticity in mice after     motoneuronal loss via sonic hedgehog signaling, immunomodulation     and metabolic rebalancing</i>	<i>p.30</i>
<b>CONCLUDING REMARKS</b>	<i>p.50</i>
<b>REFERENCES</b>	<i>p.54</i>

*PAPERS*

*p.58*

*ACKNOWLEDGEMENTS*

*p.60*

## **SUMMARY**

Amyotrophic lateral sclerosis (ALS) is a fatal neurodegenerative disease characterized by degeneration of upper and lower motoneurons. Although the main feature is motoneuronal loss, ALS is more than a motoneuronal disease, whose pathophysiology made ALS a multisystem disease, involving also non autonomous cells, particularly astrocytes, microglia and muscle cells, which altogether contribute to generate a hostile microenvironment for neurons survival. To this date, it is impossible for ALS patients to escape from death, which inevitably occurs in 3-5 years from diagnosis, considering also that the only FDA-approved drugs, such riluzole and edaravone, barely slow disease progression and increase life expectancy of just a couple of months. Transgenic mice models, for their capacity to recapitulate accurately characteristics of human ALS disease, are the most used to shed light on pathological mechanisms and uncover new therapeutic approaches. Nevertheless, new animal models should be examined, considering also that sporadic ALS is the most prevalent form. From this point of view, innovative reductionistic animal models would help to dissect step by step aspects of a such complex disease, regardless of the presence of a gene mutation.

Herein, for this PhD project we thought to characterize an experimental model of selective motoneuronal depletion induced by a toxin, referred as CTB-Sap model, and to investigate the involvement and modulation of a pathway important for regenerative and compensatory processes, which is the sonic hedgehog (Shh) signaling pathway, whose disruption has been discovered in neurodegenerative diseases including ALS.

Recent literature highlights the potential neuroprotective effects of clobetasol, a glucocorticoid FDA approved drug for dermatological conditions, which besides the principal glucocorticoid receptor-based mechanism of action, it has also been demonstrated to be able to activate the canonical Shh signaling pathway acting as an agonist of a component of the pathway, which is the coreceptor Smo. Thus, we decided to assess the effects of clobetasol in CTB-Sap motoneurons depleted mice, focusing on potential functional recovery, spinal cells and muscular cells modulation, also including metabolic reprogramming impact.

Our results demonstrate that clobetasol promotes 1) behavioral improvement reducing muscle denervation; 2) spinal cord plasticity restoring Shh signaling; 3) metabolic reprogramming and pro-inflammatory resident cells reduction in the spinal cord; 4) muscle repair and metabolic changes, with reestablished mitochondrial integrity. Collectively, we

assume that all those clobetasol induced effects in both spinal cord and muscle finally converge in an overall neuromuscular plasticity upon motoneuronal loss, thus suggesting clobetasol for potential translational drug therapy to promote compensatory and regenerative mechanisms in motoneuronal depleted diseases.



## INTRODUCTION

### *Definition and clinical features of Amyotrophic lateral sclerosis (ALS)*

Amyotrophic lateral sclerosis (ALS) is a progressive neurodegenerative disease of the adulthood characterized by degeneration of upper and lower motoneurons (MNs), respectively localized in the brain, and in the brainstem and spinal cord. Specifically, upper MNs for definition are those projecting from the cortex to the brainstem and to the spinal cord, whereas lower MNs project from the brainstem and spinal cord to the periphery, innervating muscles and allowing contraction and function (Hardiman, Al-Chalabi et al. 2017). In the classic clinical form of ALS usually we observe degeneration of both upper and lower MNs at the same time, even though it is also common to find the impairment mainly of only one of the two MNs categories in the so called “non-classical” phenotypes of the disease (Goutman, Hardiman et al. 2022).

The name of the disease originates from “amyotrophy”, which indicates a typical clinical sign of ALS patients’ muscle, which is the loss of muscle, whereas “lateral sclerosis” refers to a pathophysiological context that evolves in axonal damage in the lateral spinal cord columns, with critical consequences for innervation (Goutman, Hardiman et al. 2022). Although ALS has been considered so long a motor disease confined to neurons, nowadays such neuron-centered point of view has been abandoned to hold a new paradigm, which considers ALS as a multi-system disease, whose complexity and heterogeneity may delete and compromise diagnosis and then prognosis. Considering clinical manifestation, ALS patients generally show primary motor symptoms (related to primary MNs dysfunctions), such as muscular atrophy, muscle spasticity, and muscle weakness that usually spreads in other regions of the body (e.g. to the contralateral, rostral or caudal side) (Goutman, Hardiman et al. 2022). This condition leads over time to the paralysis of the skeletal muscles, involving also respiratory muscles which causes respiratory failure and eventually death. For this reason, patients usually have a poor prognosis with a median survival of 3-5 years since ALS diagnosis (Garcia-Garcia, Martin-Herrero et al. 2021). Furthermore, initial clinical manifestation may differ among patients, depending on the onset of the disease: in case of spinal onset, symptoms appear at distal upper and lower limbs; for bulbar onset, symptoms depend by the involvement of facial, tongue and pharyngeal muscles and include dysarthria and dysphagia (Goutman, Hardiman et al. 2022), (Hardiman, Al-Chalabi et al. 2017). Besides such purely motor symptoms, ALS patients may also experience non motor

symptoms, such as cognitive and/or behavioral impairment (i.e. frontotemporal dementia, executive dysfunction such as working memory affection, apathy, disinhibited behavior) (Goutman, Hardiman et al. 2022).

### *Epidemiology and etiology of ALS*

ALS has a global prevalence of 4.42 per 100.000 population and an incidence of 1.59 per 100.000 person-year, with both incidence and prevalence higher in men than in woman (Xu, Liu et al. 2020). Furthermore, ALS incidence and prevalence assume higher values in developed countries compared to the developing ones, due to a more comfortable lifestyle and therefore more longevity (Xu, Liu et al. 2020). The median age of disease onset is 55-60 years, without excluding manifestation cases during the early adulthood usually associated with sporadic ALS form (Brown and Al-Chalabi 2017).

Even nowadays ALS etiology is still largely unclear. The causes that underlie the occurrence of the disease derive from a complex interconnection among genetic components, which are not necessarily inherited, environmental factors (e.g. exposition to toxins, viral infections) and predisposing individual risk factors (e.g. smoking, physical activity). Conventionally, even though such definition may result reductionistic, ALS patients can be classified into familiar ALS and sporadic ALS patients, both revealing some similarity in symptoms and disease progression. Basically, familiar ALS affects a small proportion of the total ALS patients (5-10%) and it is associated with gene mutations and heritability. Sporadic ALS, which instead affects the majority of patients (about 90%), originates from a genetic susceptibility to external risk factors (Talbot, Malek et al. 2016), although gene mutations were also found. In clinical practice, familiar and sporadic forms are discriminated basing on the presence of a confirmed familiar case carrying the same disease-causing mutations (Goutman, Hardiman et al. 2022). The main gene mutations detected in ALS concern SOD1 (encoding for Cu/Zn superoxide dismutase 1, involved in oxidative stress), TARDBT (encoding for TAR-DNA-binding protein namely also TDP43, involved in RNA metabolism), FUS (encoding RNA binding protein FUS for RNA metabolism), C9orf72 (encoding for guanine nucleotide exchange C9orf72, involved in RNA metabolism and autophagy) (Hardiman, Al-Chalabi et al. 2017, Yamanaka and Komine 2018). Contrary to the fact that gene mutations involved in ALS are particularly of interest in preclinical models of ALS, it is worth noting that, besides the fact that sporadic form is most prevalent, it has also been highlighted that most of the total cases of ALS show unknown or no evident mutations (Mejzini, Flynn et al. 2019), suggesting that new preclinical models should be

required, and also that more attention should be focused on other risk components. Of note, several studies demonstrated that environmental factors and in particular neurotoxins have a role in triggering lots of neurodegenerative diseases. Particular is the case of Chamorro population living in Guam island, among whom a high incidence of ALS was found because of a process of biomagnification, due to the presence in cycad seeds of a content in  $\beta$ -N-methylamino-L-alanine (BMAA), a neurotoxin produced by cyanobacteria that causes protein misfolding and glutamate receptors activation, leading to neurotoxicity (Cox, Banack et al. 2003, Murch, Cox et al. 2004, Caller, Doolin et al. 2009).

### *Pathophysiology of ALS*

When taking a deep look into the pathophysiology of ALS, due to the multisystemic features recently attributed, it would be unlikely to ascribe a single pathogenetic mechanism. Particularly, it would be more appropriated to consider a set of pathogenetic factors contributing to the development and progression of the disease. Indeed, multiple factors have been suggested to occur, not only exclusively in MNs, but also in non-neuronal cells (glial cells, peripherally immune cells and muscle cells). Collectively, glutamate excitotoxicity, oxidative stress, mitochondrial dysfunction, disruption of RNA metabolism, axonal damage, altered protein homeostasis (i.e. folding, trafficking and degradation of proteins) cytoskeletal alteration or trafficking alteration, impaired DNA repairing processes, altogether lead to the peculiar neuropathological spectrum of ALS, although a common pathway which explains the concurrence of these phenomena at the same time remains unknown (Mejzini, Flynn et al. 2019, Le Gall, Anakor et al. 2020, Goutman, Hardiman et al. 2022).

Although more than one gap still needs to be filled, it can be certainly recognized that common hallmarks of ALS, shared also by other neurodegenerative diseases, are protein aggregation and neuroinflammation, this last mediated by reactive microglia and reactive astrocytes, which foster the toxic milieu by the release of cytokines and other pro-inflammatory mediators (Glass, Saijo et al. 2010). Of note, SOD1 aggregates and reactive gliosis have been found in ALS, comparably to  $\beta$  amyloid aggregates and microglial activation in Alzheimer's disease,  $\alpha$ -synuclein aggregates and reactive astrocytes/microglia in Parkinson's disease, and cytokines/antibodies accumulation and myeloid/lymphoid cell activation in multiple sclerosis (Glass, Saijo et al. 2010).

Traditionally defined as a disease of motoneuron cell body, the starting point of motoneuron degeneration has long been debated. An anterograde degeneration has been proposed with

the dying-forward hypothesis, according to which glutamate excitotoxicity, together with other mechanisms, initiate MNs degeneration in the cortex, and then descend and propagate peripherally, towards axons and reaching and affecting the neuromuscular junction, causing ultimately muscle denervation and motor defects. Nevertheless, it has become ever wider and increasingly accepted the evidence that pathological alterations begin distally at the neuromuscular junction level (Moloney, de Winter et al. 2014) (Campanari, Garcia-Ayllon et al. 2016, Verma, Khurana et al. 2022), at very early stages of disease, even before MNs degeneration and clinical symptoms onset. This hypothesis known as the dying-back hypothesis, considers ALS as distal axonopathy and it is consistent with Fisher et colleagues research, which demonstrated for the very first time in SOD1<sup>G93A</sup>, the most widely used transgenic model for ALS, that pathological changes establish distally at early time point before classical clinical symptoms (Fischer, Culver et al. 2004). Particularly, they found a significant denervation of endplates, that progressively causes a missing overlap with terminal axons, while motoneuronal loss was shown weeks later. Moreover, similar findings were observed in a case of familiar ALS patient, whose autopsy showed muscle denervation, consistent with electromyographic signs found before patient death, with intact MNs in the cortex instead (Fischer, Culver et al. 2004). To support a later involvement of MNs, we have to mention that electromyography still remains the gold standard to confirm ALS diagnosis (Ramroop and Cruz 2022), able to detect denervation signs in muscle at early stages and then reducing time to obtain diagnosis. Such evidence would confer a prominent and novel role for muscle cells in the physiopathology of ALS.

### *Diagnostic and therapeutic approaches*

Due to the heterogeneity in ALS clinical features manifestation and possible overlap with other neurological disorders, diagnosis may be challenging for clinicians. ALS diagnosis is mainly based on patients' clinical history (e.g. symptoms onset and progression, familiar clinical history), physical examination, differential diagnosis, together with supportive and confirmatory tests (Goutman, Hardiman et al. 2022), among which electromyography (EMG) is the most important diagnostic tool (Brown and Al-Chalabi 2017). International guidelines that would have had clarified the diagnostic approach, initially for research purposes mainly, were reunited for the first time in the El Escorial criteria, which originated from a workshop organized in 1990 by the World Federation of Neurology at El Escorial, Spain (Brooks 1994). These criteria classified the disease in four categories that described the certainty of ALS as definite, probable, possible, and suspected ALS, considering upper and lower dysfunction signs in a certain number of body regions. In 1998, such criteria were revised and updated (giving origin so to revised El Escorial criteria or Airlie House criteria), by abolishing the category of suspected ALS, introducing also the electromyographic criteria and adopting a new classification. According to such revised El Escorial criteria, clinical certainty could be categorized as clinically definite, probable, probable laboratory-supported and possible ALS. In 2008, new Awaji criteria improved sensitivity converting the restrictive fulfilment of electromyographic criteria in clinical findings observation (Talbot, Malek et al. 2016) and eliminated laboratory supported probable ALS (Shefner, Al-Chalabi et al. 2020). Over the years, with the intent to promote early diagnosis and overcome complexity of these criteria, new Gold Coast Criteria were proposed in Australia in September 2019 (Johnsen 2020). These new simplified criteria eliminated possible, probable and definite diagnostic categories (Goutman, Hardiman et al. 2022) and reduced them to ALS and not ALS (Johnsen 2020). Particularly, Gold Coast criteria define ALS by progressive motor impairment, upper and lower motoneuron dysfunction in at least one body region or lower motoneuron dysfunction in at least two body regions, and by investigative findings that exclude other diseases (Goutman, Hardiman et al. 2022) (Shefner, Al-Chalabi et al. 2020). To date, despite all efforts in the research field, there is no cure able to revert ALS. Only two Food and Drug Administration (FDA)-approved drug are available for ALS therapeutic management as disease-modifying, such as riluzole and edaravone, which merely result in slowing down disease progression. Although the exact mechanism of action still needs to

be fully clarified, they are supposed to act on the glutamatergic/excitotoxic and oxidative stress components of ALS, respectively. Specifically, riluzole, the oldest drug approved for ALS treatment in 1995 (Oskarsson, Gendron et al. 2018) (Bhandari, Kuhad et al. 2018), reduces glutamatergic transmission by the blocking of voltage-gated sodium channel on presynaptic neurons, whereas edaravone has an antioxidant activity similarly to a radical scavenger, reducing ROS-induced neuronal toxicity. However, despite edaravone got the FDA approval for ALS treatment in 2017, the approval is still missing in Europe by the European Medicines Agency (Oskarsson, Gendron et al. 2018) (Bhandari, Kuhad et al. 2018). Considering these limitations, in the absence of temporary efficient therapy able to revert or block disease course, symptomatic treatments are largely used, with the intent to manage worsening of symptoms which can compromise quality of life (Hardiman, Al-Chalabi et al. 2017).

### *Sonic hedgehog signaling pathway*

Besides the role during central nervous system development, several studies highlight that sonic hedgehog (Shh) signaling pathway also exerts a role in neuroprotective and regenerative and or compensatory processes (Belgacem, Hamilton et al. 2016).

Specifically, Shh is a glycoprotein of the hedgehog family (comprising also desert-hedgehog or Dhh and Indian hedgehog or Ihh) usually released in the central nervous system under physiological condition by neurons, and it works as a homeostatic signal for astrocytes, which have a high responsiveness to Shh, but it also can be secreted by astrocytes themselves during pathological conditions (Ugbode, Smith et al. 2017). Particularly, it has been recently found *in vitro* that Shh pathway stimulation in astrocytes with Shh agonists, modulates astrocytes phenotype, reduces neuronal firing frequency, and protects neurons from excitotoxicity in co-cultures. This phenomenon suggests that Shh signaling has a neuroprotective function through neuron-astrocytes crosstalk (Ugbode, Smith et al. 2017).

Specifically, Shh recruitment involves the binding to its 12-domains transmembrane receptor Patched (Patch), which usually exerts a tonic inhibition on the 7-domains transmembrane coreceptor Smoothed (Smo). Shh-Patch interaction promotes Smo disinhibition, which consequently activates Gli transcriptional factors (i.e. Gli1, Gli2, Gli3), leading to the activation or repression of targeted genes. This signaling cascade is named the canonical Shh signaling pathway, whereas the non-canonical does not require Gli engagement. Moreover, Gli1 is considered the main effector of the pathway and it is usually used as a marker to evaluate the state of pathway activation (Traiffort, Angot et al. 2010).

Interestingly, aberrant signaling of Shh pathway has been found in some neurodegenerative diseases (Yang, Qi et al. 2021), including ALS, proposing that modulation of the pathway may be useful to support compensatory processes upon motoneuronal loss. Particularly, one of the most important *in vivo* findings of Shh signaling pathway downregulation derives from cerebrospinal fluid of ALS patients (Drannik, Martin et al. 2017), in which Shh levels remain unaltered, whereas a significant reduction of the nuclear translocation of Gli1 has been found (Drannik, Martin et al. 2017), suggesting that upregulation of the pathway may be considered a potential therapeutic strategy in ALS, potentially through Smo targeting with Smo agonist drugs.

Among these, clobetasol, a glucocorticoid FDA approved drug for dermatological affection treatments, has been proposed as a new neuroprotective and regenerative alternative strategy (Vicario, Bernstock et al. 2019) (Najm, Madhavan et al. 2015).

*Experimental animal model of selective motoneurons depletion: CTB-Sap model*

The use of preclinical models recapitulating clinical and pathological features of ALS are crucial for both the development of new therapeutic approaches and the clarification of pathophysiological mechanisms. In this scenario, transgenic animal models are certainly the most used for ALS (Gois, Mendonca et al. 2020). However, reductionistic models, which mimic single aspects of a disease in a controlled and simplified manner, would help in better understanding key points of a such complex multi-system disease.

In this regard, cholera toxin B subunit (CTB) – saporin conjugated (Sap) model (hereafter referred as CTB-Sap model) has been used as a reductionistic experimental mouse model of selective depletion of spinal lamina IX MNs (Gulino, Vicario et al. 2019). In this model, CTB-Sap is used as a conjugated compound, thereby taking simultaneously advantage of both cholera toxin and saporin proprieties: cholera toxin acts as a moiety, driving saporin to motoneuron cell bodies through a GM1 ganglioside binding-based mechanism, whereas saporin, which alone does not enter cells, holds the neurotoxic activity, acting as a ribosome-inactivating protein, thus provoking protein synthesis block in MNs and finally conveying to apoptotic death (Llewellyn-Smith, Martin et al. 2000) (Bolshakov, Stepanichev et al. 2020). Thus, CTB-Sap is injected to selectively kill MNs. In detail, the neurotoxic complex CTB-Sap is injected into the left gastrocnemius muscle of mice, and then from periphery via retrograde axonal transport reaches motoneuron soma, within it is internalized and exerts as a final effect motoneuronal loss (Gulino, Vicario et al. 2019).



## ***AIMS OF THIS THESIS***

The general objective of this PhD thesis was to characterize a reductionistic experimental murine model of selectively depleted spinal motoneurons, namely CTB-Sap model, and evaluate potential beneficial effects of Shh pathway modulation upon motoneuronal loss, using clobetasol as a Smo-agonist and activator of the canonical signaling cascade.

More specifically, the main aims were:

- 1) Behavioral characterization of CTB-Sap model, comprising the motor impairment assessment and the electromyographic evaluation;
- 2) Pathophysiological characterization of CTB-Sap model, with a particular focus on both spontaneous CNS (glial and immune contribute which underlie concurrent neuroinflammation) and muscle response to motoneurons, including analysis of immunomodulation and metabolomics;
- 3) Investigation of Shh signaling in CTB-Sap model and clobetasol-induced modulation effects in supporting neuromuscular plasticity and compensatory processes, and in ameliorating motor impairment.

## ***RESULTS***

## Increased expression of connexin 43 in a mouse model of spinal motoneuronal loss

Federica Maria Spitale<sup>1,\*</sup>, Nunzio Vicario<sup>1,\*</sup>, Michelino Di Rosa<sup>2</sup>, Daniele Tibullo<sup>3</sup>, Michele Vecchio<sup>4,5</sup>, Rosario Gulino<sup>1</sup>, Rosalba Parenti<sup>1</sup>

<sup>1</sup>Department of Biomedical and Biotechnological Sciences, Section of Physiology, University of Catania, Catania 95123, Italy

<sup>2</sup>Department of Biomedical and Biotechnological Sciences, Section of Anatomy, Histology and Movement Sciences, University of Catania, Catania 95123, Italy

<sup>3</sup>Department of Biomedical and Biotechnological Sciences, Section of Biochemistry, University of Catania, Catania 95123, Italy

<sup>4</sup>Department of Biomedical and Biotechnological Sciences, Section of Pharmacology, University of Catania, Catania 95123, Italy

<sup>5</sup>Rehabilitation Unit, "AOU Policlinico Vittorio Emanuele", University of Catania, Catania 95123, Italy

\*Equal contribution

**Correspondence to:** Rosario Gulino, Rosalba Parenti; email: [rogulino@unict.it](mailto:rogulino@unict.it), [parenti@unict.it](mailto:parenti@unict.it)

**Keywords:** ALS, neurodegeneration, neuronal loss, astrocyte, gap junction

**Received:** April 1, 2020

**Accepted:** June 5, 2020

**Published:** June 24, 2020

**Copyright:** Spitale et al. This is an open-access article distributed under the terms of the Creative Commons Attribution License (CC BY 3.0), which permits unrestricted use, distribution, and reproduction in any medium, provided the original author and source are credited.

### ABSTRACT

Amyotrophic lateral sclerosis (ALS) is one of the most common motoneuronal disease, characterized by motoneuronal loss and progressive paralysis. Despite research efforts, ALS remains a fatal disease, with a survival of 2-5 years after disease onset. Numerous gene mutations have been correlated with both sporadic (sALS) and familiar forms of the disease, but the pathophysiological mechanisms of ALS onset and progression are still largely uncertain. However, a common profile is emerging in ALS pathological features, including misfolded protein accumulation and a cross-talk between neuroinflammatory and degenerative processes. In particular, astrocytes and microglial cells have been proposed as detrimental influencers of perineuronal microenvironment, and this role may be exerted via gap junctions (GJs)- and hemichannels (HCs)-mediated communications. Herein we investigated the role of the main astroglial GJs-forming connexin, Cx43, in human ALS and the effects of focal spinal cord motoneuronal depletion onto the resident glial cells and Cx43 levels. Our data support the hypothesis that motoneuronal depletion may affect glial activity, which in turn results in reactive Cx43 expression, further promoting neuronal suffering and degeneration.

### INTRODUCTION

Amyotrophic lateral sclerosis (ALS) is a progressive neurodegenerative disease that affects upper and lower motoneurons [1, 2]. Although the main ALS hallmark is motoneuronal loss due to motoneuron vulnerability, resident glial cells play a crucial role in ALS pathogenesis. In particular, during the disease progression, a robust neuroinflammation, glial activation and misfolded protein

accumulation can be observed, together driving progressive neuronal loss and persistent disabilities [3, 4]. Recent evidence on neurodegenerative/inflammatory disorders have highlighted a key role of neuroglial cross-talk, which substantially contributes to neuronal suffering and degeneration [3, 4].

Gap junctions (GJs) are characterized by the juxtaposition of two hemichannels (HCs) of adjacent cells, and allow the

exchange of ions, metabolites, and other mediators < 1 kDa between intracellular fluids (i.e. GJs-mediated intercellular communication) or between intracellular and extracellular compartment (i.e. HCs-mediated communication) [5, 6]. GJs are aggregates in defined plasma membrane regions of adjacent cells forming the so-called GJs plaques, in which GJs are rapidly assembled, disassembled or remodelled [6]. Previous evidence demonstrated that connexins (Cxs), the core GJs- and HCs-forming proteins, exert a prominent role in maintaining physiological functions and promoting reactive activation of glial cells [7]. Indeed, previous reports on transgenic mouse models of ALS, showed an early Cx43-reactive expression on spinal cord microenvironment. This evidence was also observed in aging and in major neurodegenerative disorders, including spinal cord injury and Alzheimer's disease [8–10]. It seems likely that ALS has a focal onset in the central nervous system, where microenvironmental conditions are particularly hostile and mediate neurodegeneration spread and progression [2, 11, 12]. Thus, we developed a mouse model of focal removal of lumbar spinal cord motoneurons using retrograde suicide transport of saporin, conjugated to cholera toxin-B subunit (CTB-Sap) [13, 14].

Herein we investigated Cx43, the most abundant GJs- and HCs-forming protein of the central nervous system, and its possible role in human ALS, as well as in the CTB-Sap model [13, 14]. We have shown that Cx43-reactive expression may represent the biological substrate underlying reactive glial activation and neuronal suffering in neurodegenerative diseases.

## RESULTS

### Correlation between GJA1 and GFAP in human ALS

We first tested the hypothesis of a potential role of Cx43 in human ALS analysing the z-score of mRNA expression levels in the central nervous system of control and sporadic (s)ALS patients. We used the NCBI Gene Expression Omnibus (GEO) database (<http://www.ncbi.nlm.nih.gov/geo/>) to select human healthy and ALS gene expression dataset. We analysed the GFAP (encoding for the glial fibrillary acidic protein) and GJA1 (encoding for Cx43) expression levels in central nervous system biopsies of healthy and sALS patients. Our analysis revealed that in sALS patients both GFAP and GJA1 mRNA levels were significantly increased as compared to the healthy counterpart (Figure 1A, 1B). We then moved to analyse a potential correlation between GFAP and GJA1 performing a linear regression analysis, finding a positive correlation between tested genes in human sALS central nervous system ( $r^2 = 0.4765$ ,  $p$ -value < 0.0001, Figure 1C).

### CTB-Sap-induced motoneuronal depletion mediates behavioural impairment in mice

In order to analyse the effects of motoneuronal loss and its impact on behavioural and neuropathological signs *in vivo*, we established a model of spinal motoneuronal depletion induced by the neuronal targeting toxin CTB-Sap, which is retrogradely transported throughout axons

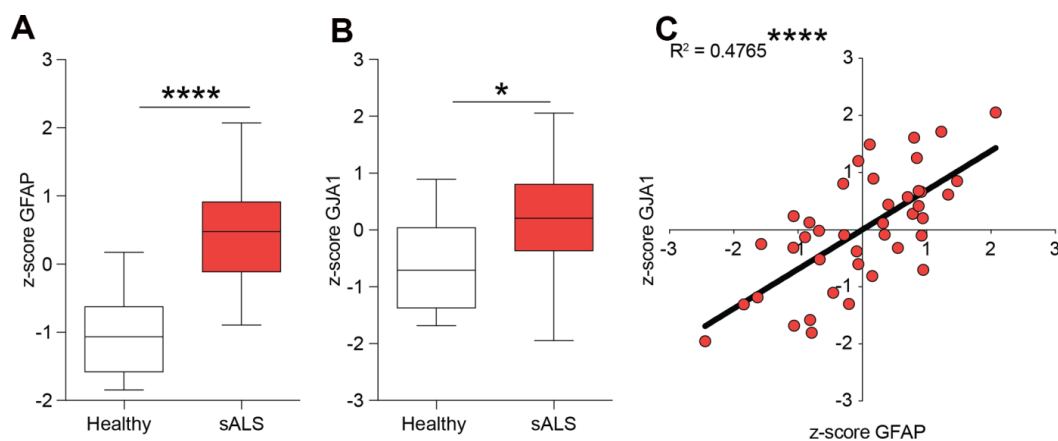


**Figure 1. Expression levels of GFAP and GJA1 encoding for Cx43 in human sALS biopsies.** (A, B) mRNA expression levels of GFAP (A) and GJA1 (B) in the central nervous system of sALS patients versus healthy control levels. Data are expressed as z-score intensity expression levels and presented via standard Box and whiskers plot. \*\*\*\* $p$ -value < 0.0001 and \* $p$ -value < 0.05 versus healthy control group. (C) Linear regression analysis of GFAP and GJA1 z-scores in sALS group.

to the spinal cord. We evaluated the behavioural impact of motoneuronal loss at 0, 7, 21 and 42 days post-lesion (dpi), performing an open field grid walk test (Figure 2A), tracking the distance covered by mice during the task with a tracking camera, and the number of footfalls over meter with a counting camera (Figure 2A). We found that both healthy control and CTB-Sap lesioned mice were active in the performance and covered an average distance of  $3.2 \pm 0.5$  and  $4.2 \pm 1.0$  meters, respectively (p-value > 0.444, Figure 2B). We also found that CTB-Sap lesioned mice showed a significant increase of the rate of errors as soon as 7 dpi and that such motor coordination impairment was retained up to 42 dpi (Figure 2C). We confirmed this evidence evaluating the clinical impairment during the time course of disease. Our data indicate that lesioned mice presented a stable impairment and a clinical score of

about 2 (Figure 2D), showing leg extension towards the lateral midline and also affected stepping during locomotion test.

### CTB-Sap induces typical electromyographic signs of denervation

In order to better characterize the denervation in CTB-Sap-injected mice, we performed an electromyographic recording into the left gastrocnemius muscle to find signs of denervation and spontaneous electrical activity. The results of our analysis are reported in Figure 3A, 3B and show that CTB-Sap induces muscle denervation, as suggested by a relevant number of positive sharp waves, fibrillations, fasciculations and neuromyotonia (Figure 3B). Of note, our electromyographic analysis found no obvious signs of myopathy.

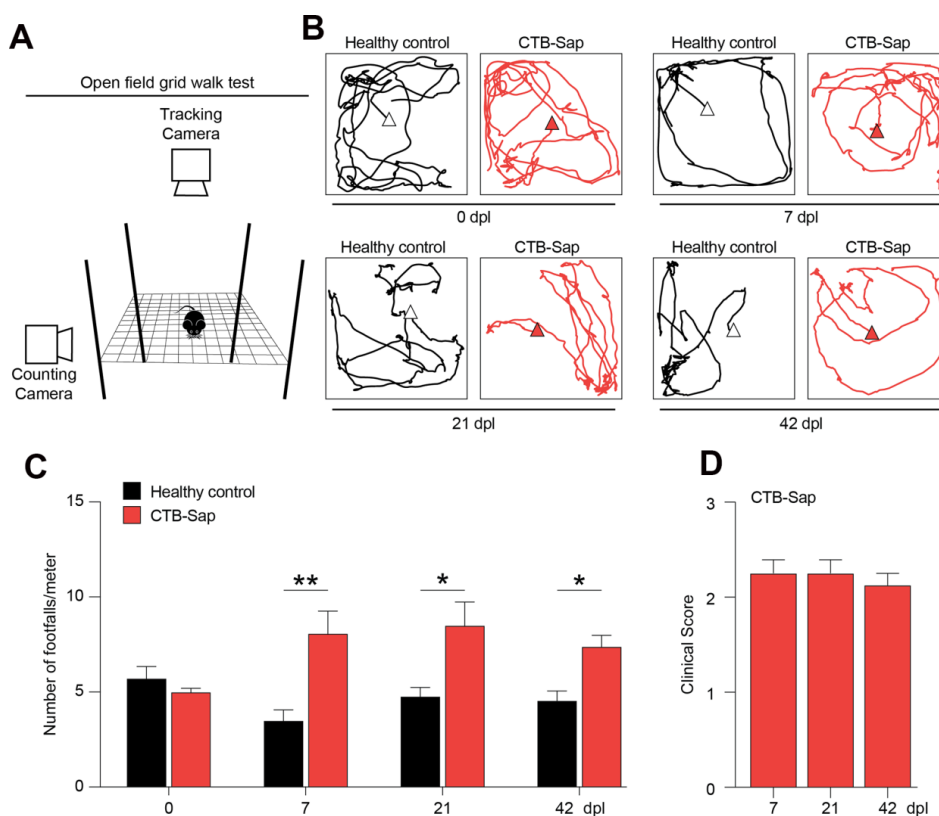


**Figure 2. Motor impairment in spinal motoneuronal depleted CTB-Sap mice.** (A) Experimental setting of open field grid walk behavioural platform. (B, C) Representative tracks (B) and quantification of the number of footfalls over meter (C) of healthy (black) and CTB-Sap lesioned (red) mice at 0, 7, 21 and 42 days post-lesion (dpi); data are mean  $\pm$  SEM; \*\*p-value < 0.01 and \*p-value < 0.05 versus healthy control group. (D) Clinical score of CTB-Sap-lesioned mice in the time course of lesion; data are mean  $\pm$  SEM.

### Spinal cord neuropathological analysis

We then moved to analyse the neuropathological effects of CTB-Sap, by quantifying the impact onto the resident motoneuronal populations. Our analysis revealed a striking reduction of left over right motoneuron number in Rexed lamina IX of CTB-Sap lesioned mice versus healthy control (Figure 3C, 3D). This depletion is also evident in Figure 3D, which shows representative images of cresyl violet-positive

motoneurons in left Rexed lamina IX of healthy control and CTB-Sap mice.

### Cx43-mediated coupling in Rexed lamina IX glial cells

The relevance of astroglial Cx43 in human ALS prompted us to evaluate a potential involvement of this Cx in a reductionist model of spinal motoneuronal loss induced by CTB-Sap. We assessed Cx43 expression in our model, by measuring the Cx43 mean fluorescence

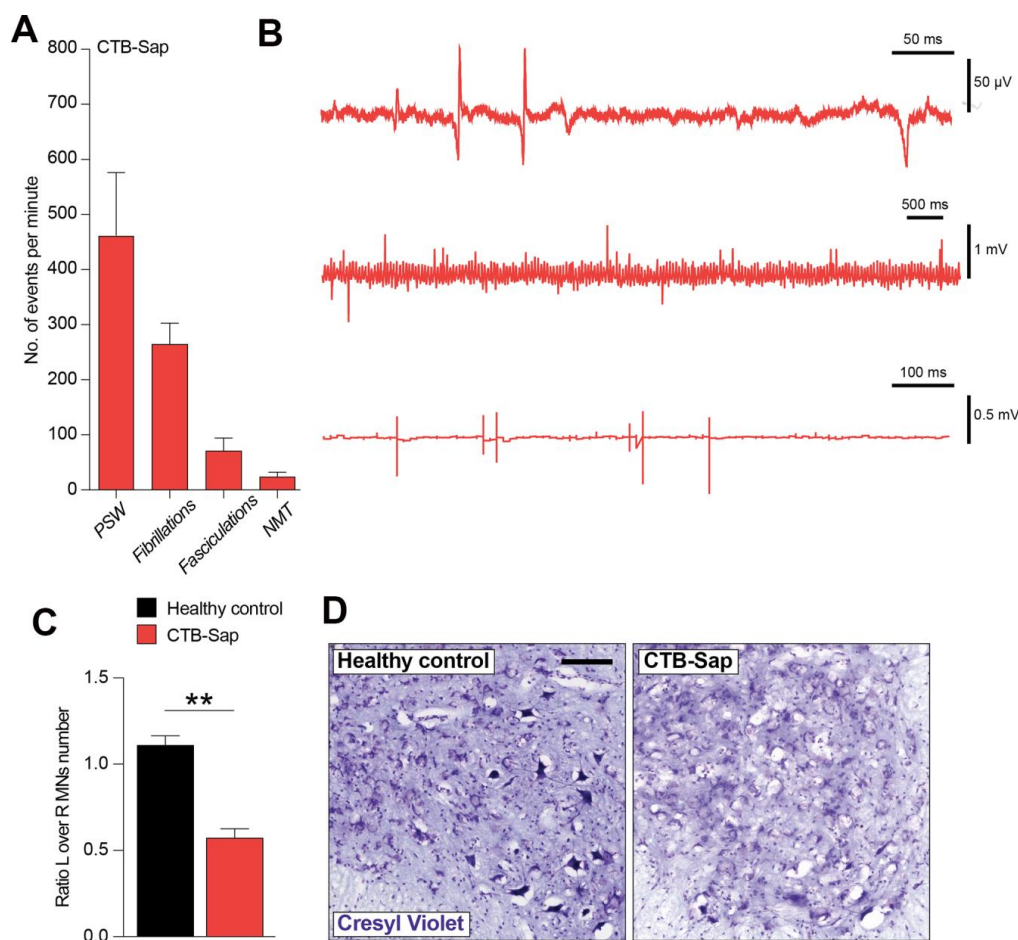


**Figure 3. Electromyographic signs and neuropathological analysis of CTB-Sap lesioned mice.** Quantification (A) and representative profile of electromyographic activity of gastrocnemius muscle in CTB-Sap lesioned mice. (B) positive sharp waves (PSW), fibrillations, fasciculation and neuromyotonia (NMT); data in (A) are expressed as mean events per minute  $\pm$  SEM. (C) Quantification of the number of neurons in left (L) over right (R) ventral horn of CTB-Sap lesioned mice versus healthy control; data are expressed as mean ratio L over R  $\pm$  SEM; \*\*p-value < 0.01 versus healthy control. (D) Representative images of cresyl violet stained motoneurons in left Rexed lamina IX of healthy control and CTB-Sap lesioned mice. Scale bar: 100  $\mu$ m. MNs: motoneurons.

intensity (MFI) in the spinal cord of healthy control and CTB-Sap mice, finding a significant MFI increase in GFAP and Cx43 levels in Rexed lamina IX of motoneuron depleted spinal cord (Figure 4A, 4B). Such an increase was coupled with morphological changes in astroglial (i.e. GFAP positive) and

microglial (i.e. IBA1 positive) cell populations (Figure 4B). Finally, we analysed the profile plot of GFAP, IBA1 and Cx43 in the spinal cord of healthy control (Figure 5A) and CTB-Sap-lesioned (Figure 5B) mice, confirming an increased colocalization between Cx43 and GFAP/IBA1 (Figure 5A, 5B).

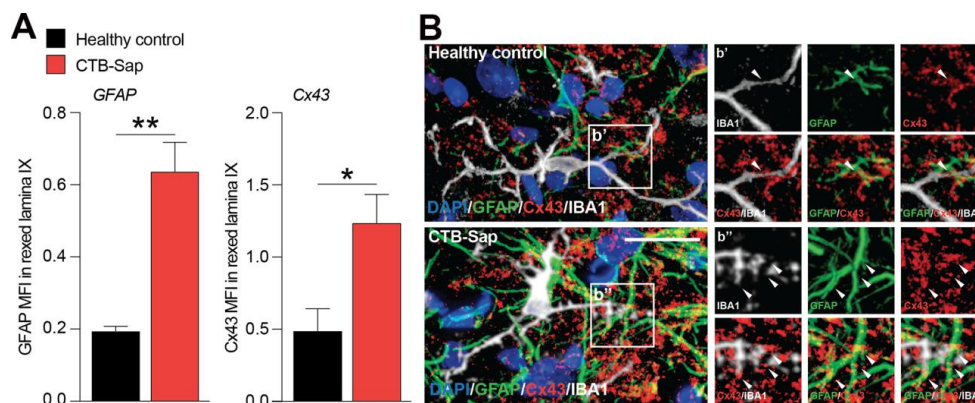


**Figure 4. Increase of Cx43 in the spinal cord cell populations of motoneuron-depleted spinal cord.** (A) Quantification of mean fluorescence intensity (MFI) of GFAP and Cx43 in the left lamina IX of healthy control and CTB-Sap lesioned mice; data are expressed as mean  $\pm$  SEM; \*\*p-value < 0.01 and \*p-value < 0.05 versus healthy control. (B) Representative confocal images of Cx43 (red) immunofluorescence analysis in lamina IX of healthy control and CTB-Sap lesioned mice; images show also markers for astroglial cells (GFAP, green) and microglia (IBA1, white); scale bar 20  $\mu$ m.

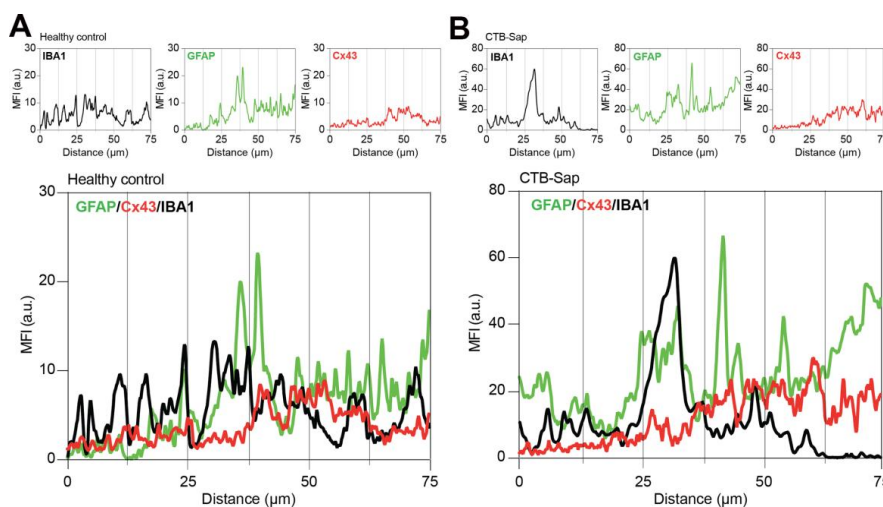


**Figure 5. Cx43-based channels profile in microglial/astroglial milieu in motoneuron-depleted spinal cord.** Profile plot of MFI of IBA1 (black plot), GFAP (green plot), and Cx43 (red plot) and plots overlay (bottom panel) in Rexed lamina IX of healthy control (A) and CTB-Sap lesioned mice (B); data are MFI arbitrary units (a.u.) of spinal confocal acquisitions.

## DISCUSSION

It is known that glial cells, both astrocytes and microglia, hold key physiological roles in the central nervous system, such as immunological surveillance, blood brain barrier function, synaptic activity, neuronal trophism and metabolic support [1, 14–18]. In the last decades, advances have come to suggest a critical role of neuroglial cross-talk and related microenvironmental modulation during neurodegenerative disorders [7, 19, 20]. Such a role, besides being an attractive target due to its pathophysiological importance, also opens new scenarios to develop potential effective therapeutic strategies.

Several *in vitro* and *in vivo* models of main neurological conditions such as stroke, multiple sclerosis, Alzheimer's disease and ALS, demonstrated that reactive astrocytes and microglia amplify neuroinflammation and neurodegeneration through aberrant GJs/HCs communication [21]. It is noteworthy that even in aging models, dysregulation of astroglial population and Cx43 dynamic expression profile may be one of the responsible mechanisms for A $\beta$  deposits in the brain [9, 22, 23].

Notably, an abnormal increase in Cx43 expression has been described as one of the mechanisms for astrocyte-mediated toxicity in both SOD1(G93A) mice and in the central nervous system of ALS patients [20].

Herein, we first analysed available data on NCBI GEO database to select human ALS transcriptome dataset (E-MTAB-2325) in order to verify whether astrogliosis and reactive Cx43 expression, which are both reported in ALS neuropathology, were positively correlated. Such analysis suggested that astrocytes represent the leading cell population in showing Cx43 expression, and that human astroglial reactive Cx43 finds a correspondence in mice model of motoneuronal diseases. Astroglial cells are able to communicate with each other through Cxs-based GJs, mainly expressing Cx43 [7]. This direct astrocyte-to-astrocyte communication is involved in homeostatic processes within the complex intercellular network they form, allowing metabolites, small molecules and second messengers trafficking. During neurodegenerative disease, central nervous system microenvironment is substantially affected by inflammatory cytokines released by reactive microglia also acting on astroglial cells. Astrogliosis and concomitant reactive Cx43 expression contribute to homocellular and heterocellular communication, also releasing reactive oxygen species and inflammatory mediators. Therefore, such unbalanced communication fosters neurotoxic and proinflammatory loop of neurodegenerative disease [24, 25].

We also assessed a toxin-based model of motoneuronal depletion established using CTB-Sap [14, 26, 27], which selectively targets axon terminals and kills motoneurons by retrograde suicide transport [28, 29], thus inducing both muscular denervation and behavioural impairment of motor performance. Our reductionist *in vivo* model of motoneuronal disorders showed functional deficits and electromyographic signs typical of both transgenic ALS mouse model and human ALS patients [30–32]. In particular, our electromyography data revealed that CTB-Sap-induced motoneuronal ablation does not induce myopathy. Indeed, no obvious signs of myopathy were found in motoneuronal depleted mice. In myopathic diseases, in addition to apparent fibrillation potentials and positive sharp waves, normal or early recruitment is found, whereas in our animal model we found profuse fibrillation potentials and positive sharp waves associated with reduced recruitment, that is a typical pattern found in neuropathy and also observed in ALS patients [33, 34].

In CTB-Sap induced motoneuronal depletion, we have therefore observed typical ALS electromyographic signs of denervation, thus supporting this model as a valuable tool to study neurodegeneration and central effects of reduced motoneuronal pool.

A significant aspect of our model is the evidence of reactive astrocytes expressing Cx43, which suggested an increase in intercellular communication. Our evidence does not support a relationship between neuronal ablation efficiency and glial cells activation, although a potential relationship between spared motoneurons modulating the activation and function of both microglia and astrocytes, may occur. Moreover, enhanced Cx43 expression also activates a positive-loop conditioning ventral horn microenvironment that likely exerts a detrimental effect on spared motoneurons. Accordingly, negative effects induced by Cx43 overexpression have been reported in experimental models of ALS, showing that increased glial Cx43-channels significantly affect neuronal activity and wellness [20]. In particular, experimental evidence supports the hypothesis that Cx43 could exert such a detrimental role when assembled as HCs and exposed to cell membrane. Such an effect may be linked to increased excitotoxic calcium release, reactive oxygen species, glutamate and ATP, thus further inducing neuronal distress and death [1, 25, 35–37]. The role of microglial cells during neurodegeneration is also of importance, in particular for their role as master regulators of inflammatory cytokine release. Microglia modulates astroglial functions releasing IL-1 $\beta$  and TNF $\alpha$  that have been linked to an overall increase of Cx43-based HCs activity, further sustaining neuronal suffering [38, 39].



In the present report, we found an altered glial activity in an experimental model of motoneuronal depletion, resulting in a reactive Cx43 expression. Further studies will help to characterize the molecular mediators and the role of selective silencing and/or pharmacological modulation of Cx43 function. GJs- or HCs-forming protein in CTB-Sap induced focal motoneuronal depletion may also offer the opportunity to evaluate a potential discrepancy of Cx43 biological meaning in the early versus the late stage of disease. Crucial information may be derived by Cx43 knockout models upon neurodegenerative insults, even if potential cross-modulation among Cxs may take place. Of note, the role of microglial GJs and HCs is still matter of debate, in particular on the heterocellular (i.e. microglia-astrocytes) GJs composition. A deeper investigation on the role of Cx43 in microglial cell population and on the crucial role of HCs in neuroglial crosstalk will help to elucidate biological substrates and to highlight potential therapeutic targets in neurodegenerative diseases.

## MATERIALS AND METHODS

### Human ALS data

For human ALS data, we used the NCBI Gene Expression Omnibus (GEO) database (<http://www.ncbi.nlm.nih.gov/geo/>) to select human ALS central nervous system transcriptome dataset (E-MTAB-2325) analysing the GFAP (encoding for the glial fibrillary acidic protein) and GJA1 (encoding for Cx43) expression levels. Mesh terms “central nervous system”, “ALS” and “Human” were used to identify potential datasets of interest. Healthy control tissues were matched for age, post-mortem (PM) delay and central nervous system region. The samples characteristics are available in Table 1. The analysis of microarray data by Z-score transformation was performed using MultiExperiment Viewer (MeV) software (The Institute for Genomic Research (TIGR), J. Craig Venter Institute, USA), in order to allow the comparison of microarray data independent of the original hybridization intensities and reduce the noise of original intensity signal [40–42].

### Animal model

All experiments were performed in accordance with the principle of the Basel Declaration as well as with the European Communities Council directive and Italian regulations (EEC Council 2010/63/EU and Italian D.Lgs. no. 26/2014). The protocol was approved by the Italian Ministry of Health (auth. no. 1133/2016-PR). All efforts were made to replace, reduce, and refine the use of laboratory animals. Experiments were performed on 8–12 weeks old male 129S2/SvPasCrl (Charles River Laboratories, Calco, Italy), as previously described

[13, 14]. Briefly, a total number of 16 animals were used in this study, randomly assigned to the HC group (n = 8) or the CTB-Sap (12 µg injected into the left gastrocnemius muscle) lesioned group (n = 8). For CTB-Sap injection, mice were anesthetized with isoflurane (4% for induction, 2% for maintenance). Mice were then observed for up to 42 days post lesion (dpl) evaluating the clinical score based on the following criteria: 0 = healthy; 1 = collapse or partial collapse of leg extension towards the lateral midline during the tail suspension test; 2 = toes curl under at least twice during walking of 30 cm or any part of the foot is dragging along the cage bottom/table; 3 = rigid paralysis or minimal joint movement, foot not being used for generating forward motion; 4 = mouse cannot straighten itself within 30 s after being placed on either side.

### Electromyography

Electromyographic recording was performed as previously described [14]. Briefly, at 42 dpl mice were anesthetized with isoflurane and CTB-Sap injected gastrocnemius muscle was exposed and examined by a portable two-channel EMG device (Myoquick, Micromed S.p.A., Mogliano Veneto, Treviso, Italy) using 1 bipolar concentric needle electrode inserted in the gastrocnemius and 1 grounded electrode.

### Open field grid walk test

Open field grid walk test was performed at 0, 7, 21, and 42 dpl using a platform equipped with a tracking camera and a counting camera. Animals were placed in the arena and were free to move and to explore during the behavioural test. Each performance was recorded for 2 minutes and matched tracking and counting video were analysed off-line using Ctrax tracker software version 0.5.18 for Mac.

### Ex vivo tissue processing

At 42 dpl, spinal cord isolation, cryo-sectioning and immunofluorescence analysis were performed as previously described [43]. Briefly, isolated spinal cords were post-fixed with 4% paraformaldehyde overnight at 4 °C. Samples were then cryo-protected with 30% sucrose in PBS overnight at 4 °C and then embedded in Optimum Cutting Temperature medium. Embedded samples were snap frozen in liquid nitrogen and cut into 20 µm-thick cryosections. Sections were collected on SuperFrost slides and stored at - 80 °C until use. Before performing experiments, sections were dried at room temperature for 45 minutes and then washed in depthH<sub>2</sub>O and PBS 2 times for 5 minutes at room temperature.

**Table 1. Characteristics of healthy control and sALS human samples.**

Sample	Age	Male	Female
Healthy control	55.1±14.4	9	1
ALS	56.70±9.94	20	11

### Cresyl violet

For cresyl violet staining, spinal cord sections were dehydrated with increasing ethanol (70%, 95% 100%) in deph<sub>2</sub>O for 3 minutes and then in xylene for 5 minutes. Dehydrated sections were then homogeneously rehydrated and stained with a solution of 0.2% sodium acetate, 1% cresyl violet, 3% glacial acetic acid in deph<sub>2</sub>O for 10 min at room temperature. Sections were then washed in water, dehydrated in increasing ethanol concentrations, clarified in xylene and coverslipped.

### Immunofluorescence

Immunofluorescence was performed as previously described [43–46]. Briefly, samples were incubated overnight at 4 °C with mouse monoclonal anti-GFAP (BD Biosciences, Cat# 610566, RRID: AB\_397916, 1:500), rabbit polyclonal anti-Cx43 (Cell Signaling Technology, Cat# 3512, RRID: AB\_2294590, 1:200), goat polyclonal anti-IBA1 (Novus Biologicals, Cat# NB100-1028, RRID: AB\_521594, 1:500). The following day, sections were washed in 0.1% Triton X-100 in PBS 3 times at room temperature and then incubated 1 hr at room temperature with appropriate combination of secondary antibodies: goat polyclonal anti-mouse (Alexa Fluor 488, Thermo Fisher Scientific, Cat# A-11001, RRID: AB\_2534069, 1:1'000), goat polyclonal anti-rabbit (Alexa Fluor 564, Molecular Probes, Cat# A-11010, RRID: AB\_143156, 1:1'000) and donkey anti-goat (Alexa Fluor 647, Thermo Fisher Scientific, Cat# A-21447, RRID: AB\_2535864). Nuclei were counterstained with DAPI (1:10'000, Invitrogen) for 5 min at room temperature and then mounted with BrightMount mounting medium (Abcam). Profile plots for immunofluorescence images were obtained as previously described [43].

### Statistical analysis

All tests were performed in GraphPad Prism (version 5.00, GraphPad Software) or RStudio (version 1.0.153, RStudio Inc.). Data were tested for normality using a D'Agostino and Pearson omnibus normality test and subsequently assessed for homogeneity of variance. Data that passed both tests were further analyzed by two-tailed unpaired Student's t-test for comparison of n = 2 groups. For comparison of n ≥ 3 groups, one-way or two-way ANOVA was used where appropriate, and

associations between variables were analysed by linear regression and correlation.

### AUTHOR CONTRIBUTIONS

Conceptualization: NV, RG, RP; Investigation: FMS, NV, MDR, DT, MV, RG, RP; Formal analysis: FMS, NV, MDR, DT, MV, RG, RP; Data curation: FMS, NV; Writing the original draft: NV, RG, RP; Writing reviewing and editing: NV, FMS, NV, MDR, DT, MV, RG, RP.

### CONFLICTS OF INTEREST

Authors declare no conflicts of interest.

### FUNDING

F.M.S. was supported by the international PhD program in Neuroscience and PO FSE 2014-2020 fellow (Biometec, University of Catania, Italy). N.V. was supported by the PON AIM R&I 2014-2020 - E66C18001240007. The research was partially supported by a grant from the Italian Ministero dell'Istruzione, dell'Università e della Ricerca, PRIN 2015, Grant no.: 2015MJBEM2\_006 to R.G. The research was partially supported by a grant from the Italian Ministero dell'Istruzione, dell'Università e della Ricerca, PBCT PRIN 2017, Grant no.: 2017XKWWK9 to R.P.

### REFERENCES

- Glass CK, Saijo K, Winner B, Marchetto MC, Gage FH. Mechanisms underlying inflammation in neurodegeneration. *Cell*. 2010; 140:918–34. <https://doi.org/10.1016/j.cell.2010.02.016> PMID:20303880
- Gordon PH. Amyotrophic lateral sclerosis: an update for 2013 clinical features, pathophysiology, management and therapeutic trials. *Aging Dis*. 2013; 4:295–310. <https://doi.org/10.14336/AD.2013.0400295> PMID:24124634
- Turner MR, Hardiman O, Benatar M, Brooks BR, Chio A, de Carvalho M, Ince PG, Lin C, Miller RG, Mitsumoto H, Nicholson G, Ravits J, Shaw PJ, et al. Controversies and priorities in amyotrophic lateral sclerosis. *Lancet*

- Neurol. 2013; 12:310–22.  
[https://doi.org/10.1016/S1474-4422\(13\)70036-X](https://doi.org/10.1016/S1474-4422(13)70036-X)  
 PMID:23415570
4. McGeer PL, McGeer EG. Inflammatory processes in amyotrophic lateral sclerosis. *Muscle Nerve*. 2002; 26:459–70.  
<https://doi.org/10.1002/mus.10191> PMID:12362410
  5. Willecke K, Eiberger J, Degen J, Eckardt D, Romualdi A, Güldenagel M, Deutsch U, Söhl G. Structural and functional diversity of connexin genes in the mouse and human genome. *Biol Chem*. 2002; 383:725–37.  
<https://doi.org/10.1515/BC.2002.076>  
 PMID:12108537
  6. Gaietta G, Deerinck TJ, Adams SR, Bouwer J, Tour O, Laird DW, Sosinsky GE, Tsien RY, Ellisman MH. Multicolor and electron microscopic imaging of connexin trafficking. *Science*. 2002; 296:503–07.  
<https://doi.org/10.1126/science.1068793>  
 PMID:11964472
  7. Vicario N, Zappalà A, Calabrese G, Gulino R, Parenti C, Gulisano M, Parenti R. Connexins in the central nervous system: physiological traits and neuroprotective targets. *Front Physiol*. 2017; 8:1060.  
<https://doi.org/10.3389/fphys.2017.01060>  
 PMID:29326598
  8. Howland DS, Liu J, She Y, Goad B, Maragakis NJ, Kim B, Erickson J, Kulik J, DeVito L, Psaltis G, DeGennaro LJ, Cleveland DW, Rothstein JD. Focal loss of the glutamate transporter EAAT2 in a transgenic rat model of SOD1 mutant-mediated amyotrophic lateral sclerosis (ALS). *Proc Natl Acad Sci USA*. 2002; 99:1604–09.  
<https://doi.org/10.1073/pnas.032539299>  
 PMID:11818550
  9. Koulakoff A, Mei X, Orellana JA, Sáez JC, Giaume C. Glial connexin expression and function in the context of alzheimer's disease. *Biochim Biophys Acta*. 2012; 1818:2048–57.  
<https://doi.org/10.1016/j.bbamem.2011.10.001>  
 PMID:22008509
  10. Middeldorp J, Hol EM. GFAP in health and disease. *Prog Neurobiol*. 2011; 93:421–43.  
<https://doi.org/10.1016/j.pneurobio.2011.01.005>  
 PMID:21219963
  11. Hardiman O, Al-Chalabi A, Chio A, Corr EM, Logroscino G, Robberecht W, Shaw PJ, Simmons Z, van den Berg LH. Amyotrophic lateral sclerosis. *Nat Rev Dis Primers*. 2017; 3:17071.  
<https://doi.org/10.1038/nrdp.2017.71>  
 PMID:28980624
  12. Körner S, Kollwe K, Fahlbusch M, Zapf A, Dengler R, Krampfl K, Petri S. Onset and spreading patterns of upper and lower motor neuron symptoms in amyotrophic lateral sclerosis. *Muscle Nerve*. 2011; 43:636–42.  
<https://doi.org/10.1002/mus.21936>  
 PMID:21484822
  13. Gulino R, Perciavalle V, Gulisano M. Expression of cell fate determinants and plastic changes after neurotoxic lesion of adult mice spinal cord by cholera toxin-B saporin. *Eur J Neurosci*. 2010; 31:1423–34.  
<https://doi.org/10.1111/j.1460-9568.2010.07170.x>  
 PMID:20384775
  14. Gulino R, Vicario N, Giunta MA, Spoto G, Calabrese G, Vecchio M, Gulisano M, Leanza G, Parenti R. Neuromuscular plasticity in a mouse neurotoxic model of spinal motoneuronal loss. *Int J Mol Sci*. 2019; 20:1500.  
<https://doi.org/10.3390/ijms20061500>  
 PMID:30917493
  15. Stephenson J, Nutma E, van der Valk P, Amor S. Inflammation in CNS neurodegenerative diseases. *Immunology*. 2018; 154:204–19.  
<https://doi.org/10.1111/imm.12922>  
 PMID:29513402
  16. Cicirata F, Parenti R, Spinella F, Giglio S, Tuorto F, Zuffardi O, Gulisano M. Genomic organization and chromosomal localization of the mouse Connexin36 (mCx36) gene. *Gene*. 2000; 2:123-130.  
[https://doi.org/10.1016/s0378-1119\(00\)00202-x](https://doi.org/10.1016/s0378-1119(00)00202-x)  
 PMID:10876089
  17. Baker SM, Kim N, Gumpert AM, Segretain D, Falk MM. Acute internalization of gap junctions in vascular endothelial cells in response to inflammatory mediator-induced g-protein coupled receptor activation. *FEBS Lett*. 2008; 582:4039–46.  
<https://doi.org/10.1016/j.febslet.2008.10.043>  
 PMID:18992245
  18. Thuringer D. The vascular endothelial growth factor-induced disruption of gap junctions is relayed by an autocrine communication via ATP release in coronary capillary endothelium. *Ann N Y Acad Sci*. 2004; 1030:14–27.  
<https://doi.org/10.1196/annals.1329.003>  
 PMID:15659776
  19. Yamanaka K, Chun SJ, Boillee S, Fujimori-Tonou N, Yamashita H, Gutmann DH, Takahashi R, Misawa H, Cleveland DW. Astrocytes as determinants of disease progression in inherited amyotrophic lateral sclerosis. *Nat Neurosci*. 2008; 11:251–53.  
<https://doi.org/10.1038/nn2047>  
 PMID:18246065

20. Almad AA, Doreswamy A, Gross SK, Richard JP, Huo Y, Haughey N, Maragakis NJ. Connexin 43 in astrocytes contributes to motor neuron toxicity in amyotrophic lateral sclerosis. *Glia*. 2016; 64:1154–69. <https://doi.org/10.1002/glia.22989> PMID:27083773
21. Takeuchi H, Suzumura A. Gap junctions and hemichannels composed of connexins: potential therapeutic targets for neurodegenerative diseases. *Front Cell Neurosci*. 2014; 8:189. <https://doi.org/10.3389/fncel.2014.00189> PMID:25228858
22. Cotrina ML, Gao Q, Lin JH, Nedergaard M. Expression and function of astrocytic gap junctions in aging. *Brain Res*. 2001; 901:55–61. [https://doi.org/10.1016/s0006-8993\(01\)02258-2](https://doi.org/10.1016/s0006-8993(01)02258-2) PMID:11368950
23. Bronzuoli MR, Facchinetti R, Valenza M, Cassano T, Steardo L, Scuderi C. Astrocyte function is affected by aging and not alzheimer's disease: a preliminary investigation in hippocampi of 3xTg-AD mice. *Front Pharmacol*. 2019; 10:644. <https://doi.org/10.3389/fphar.2019.00644> PMID:31244658
24. De Bock M, Wang N, Bol M, Decrock E, Ponsaerts R, Bultynck G, Dupont G, Leybaert L. Connexin 43 hemichannels contribute to cytoplasmic Ca<sup>2+</sup> oscillations by providing a bimodal Ca<sup>2+</sup>-dependent Ca<sup>2+</sup> entry pathway. *J Biol Chem*. 2012; 287:12250–66. <https://doi.org/10.1074/jbc.M111.299610> PMID:22351781
25. Takeuchi H, Mizoguchi H, Doi Y, Jin S, Noda M, Liang J, Li H, Zhou Y, Mori R, Yasuoka S, Li E, Parajuli B, Kawanokuchi J, et al. Blockade of gap junction hemichannel suppresses disease progression in mouse models of amyotrophic lateral sclerosis and alzheimer's disease. *PLoS One*. 2011; 6:e21108. <https://doi.org/10.1371/journal.pone.0021108> PMID:21712989
26. Lind LA, Murphy ER, Lever TE, Nichols NL. Hypoglossal motor neuron death via intralingual CTB-saporin (CTB-SAP) injections mimic aspects of amyotrophic lateral sclerosis (ALS) related to dysphagia. *Neuroscience*. 2018; 390:303–16. <https://doi.org/10.1016/j.neuroscience.2018.08.026> PMID:30179644
27. Nichols NL, Craig TA, Tanner MA. Phrenic long-term facilitation following intrapleural CTB-SAP-induced respiratory motor neuron death. *Respir Physiol Neurobiol*. 2018; 256:43–49. <https://doi.org/10.1016/j.resp.2017.08.003> PMID:28822818
28. Llewellyn-Smith IJ, Martin CL, Arnolda LF, Minson JB. Tracer-toxins: cholera toxin b-saporin as a model. *J Neurosci Methods*. 2000; 103:83–90. [https://doi.org/10.1016/s0165-0270\(00\)00298-3](https://doi.org/10.1016/s0165-0270(00)00298-3) PMID:11074098
29. Wiley RG, Kline IV RH. Neuronal lesioning with axonally transported toxins. *J Neurosci Methods*. 2000; 103:73–82. [https://doi.org/10.1016/s0165-0270\(00\)00297-1](https://doi.org/10.1016/s0165-0270(00)00297-1) PMID:11074097
30. Mills KR. The basics of electromyography. *J Neurolog Neurosurg Psychiatry*. 2005 (Suppl 2); 76:ii32–35. <https://doi.org/10.1136/innp.2005.069211> PMID:15961866
31. Hadzipasic M, Ni W, Nagy M, Steenrod N, McGinley MJ, Kaushal A, Thomas E, McCormick DA, Horwich AL. Reduced high-frequency motor neuron firing, EMG fractionation, and gait variability in awake walking ALS mice. *Proc Natl Acad Sci USA*. 2016; 113:E7600–09. <https://doi.org/10.1073/pnas.1616832113> PMID:27821773
32. Quinlan KA, Kajtaz E, Ciolino JD, Imhoff-Manuel RD, Tresch MC, Heckman CJ, Tysseling VM. Chronic electromyograms in treadmill running SOD1 mice reveal early changes in muscle activation. *J Physiol*. 2017; 595:5387–400. <https://doi.org/10.1113/JP274170> PMID:28543166
33. Goutman SA. Diagnosis and clinical management of amyotrophic lateral sclerosis and other motor neuron disorders. *Continuum (Minneapolis Minn)*. 2017; 23:1332–59. <https://doi.org/10.1212/CON.0000000000000535> PMID:28968365
34. Preston DC, Shapiro BE. Electromyography and neuromuscular disorders: clinical-electrophysiologic correlations. 2005. Butterworth-Heinemann.
35. Abudara V, Roux L, Dallérac G, Matias I, Dulong J, Mothet JP, Rouach N, Giaume C. Activated microglia impairs neuroglial interaction by opening Cx43 hemichannels in hippocampal astrocytes. *Glia*. 2015; 63:795–811. <https://doi.org/10.1002/glia.22785> PMID:25643695
36. De Bock M, Wang N, Decrock E, Bol M, Gadicherla AK, Culot M, Cecchelli R, Bultynck G, Leybaert L. Endothelial calcium dynamics, connexin channels and blood-brain barrier function. *Prog Neurobiol*. 2013; 108:1–20. <https://doi.org/10.1016/j.pneurobio.2013.06.001> PMID:23851106
37. Orellana JA, Sánchez HA, Schalper KA, Figueroa V, Sáez

- JC. Regulation of intercellular calcium signaling through calcium interactions with connexin-based channels. *Adv Exp Med Biol.* 2012; 740:777–94.  
[https://doi.org/10.1007/978-94-007-2888-2\\_34](https://doi.org/10.1007/978-94-007-2888-2_34)  
 PMID:22453969
38. Froger N, Orellana JA, Calvo CF, Amigou E, Kozoriz MG, Naus CC, Sáez JC, Giaume C. Inhibition of cytokine-induced connexin43 hemichannel activity in astrocytes is neuroprotective. *Mol Cell Neurosci.* 2010; 45:37–46.  
<https://doi.org/10.1016/j.mcn.2010.05.007>  
 PMID:20684043
39. Morello G, Spampinato AG, Cavallaro S. Neuroinflammation and ALS: transcriptomic insights into molecular disease mechanisms and therapeutic targets. *Mediators Inflamm.* 2017; 2017:7070469.  
<https://doi.org/10.1155/2017/7070469>  
 PMID:29081603
40. Cheadle C, Vawter MP, Freed WJ, Becker KG. Analysis of microarray data using Z score transformation. *J Mol Diagn.* 2003; 5:73–81.  
[https://doi.org/10.1016/S1525-1578\(10\)60455-2](https://doi.org/10.1016/S1525-1578(10)60455-2)  
 PMID:12707371
41. Di Mauro R, Cantarella G, Bernardini R, Di Rosa M, Barbagallo I, Distefano A, Longhitano L, Vicario N, Nicolosi D, Lazzarino G, Tibullo D, Gulino ME, Spampinato M, et al. The biochemical and pharmacological properties of ozone: the smell of protection in acute and chronic diseases. *Int J Mol Sci.* 2019; 20:634.  
<https://doi.org/10.3390/ijms20030634>  
 PMID:30717203
42. Sanfilippo C, Castrogiovanni P, Imbesi R, Tibullo D, Li Volti G, Barbagallo I, Vicario N, Musumeci G, Di Rosa M. Middle-aged healthy women and Alzheimer's disease patients present an overlapping of brain cell transcriptional profile. *Neuroscience.* 2019; 406:333–44.  
<https://doi.org/10.1016/j.neuroscience.2019.03.008>  
 PMID:30872162
43. Vicario N, Pasquinucci L, Spitale FM, Chiechio S, Turnaturi R, Caraci F, Tibullo D, Avola R, Gulino R, Parenti R, Parenti C. Simultaneous activation of mu and delta opioid receptors reduces allodynia and astrocytic connexin 43 in an animal model of neuropathic pain. *Mol Neurobiol.* 2019; 56:7338–54.  
<https://doi.org/10.1007/s12035-019-1607-1>  
 PMID:31030416
44. Vicario N, Bernstock JD, Spitale FM, Giallongo C, Giunta MA, Li Volti G, Gulisano M, Leanza G, Tibullo D, Parenti R, Gulino R. Clobetasol modulates adult neural stem cell growth via canonical hedgehog pathway activation. *Int J Mol Sci.* 2019; 20:1991.  
<https://doi.org/10.3390/ijms20081991>  
 PMID:31018557
45. Vicario N, Calabrese G, Zappalà A, Parenti C, Forte S, Graziano AC, Vanella L, Pellitteri R, Cardile V, Parenti R. Inhibition of Cx43 mediates protective effects on hypoxic/reoxygenated human neuroblastoma cells. *J Cell Mol Med.* 2017; 21:2563–72.  
<https://doi.org/10.1111/jcmm.13177>  
 PMID:28488330
46. Mauri E, Sacchetti A, Vicario N, Peruzzotti-Jametti L, Rossi F, Pluchino S. Evaluation of RGD functionalization in hybrid hydrogels as 3D neural stem cell culture systems. *Biomater Sci.* 2018; 6:501–10.  
<https://doi.org/10.1039/c7bm01056g>  
 PMID:29368775

## ARTICLE OPEN



# Clobetasol promotes neuromuscular plasticity in mice after motoneuronal loss via sonic hedgehog signaling, immunomodulation and metabolic rebalancing

Nunzio Vicario<sup>1,2,15</sup>, Federica M. Spitale<sup>1,15</sup>, Daniele Tibullo<sup>3,15</sup>, Cesarina Giallongo<sup>4</sup>, Angela M. Amorini<sup>3</sup>, Grazia Scandura<sup>1,4</sup>, Graziana Spoto<sup>1</sup>, Miriam W. Saab<sup>3</sup>, Simona D'Aprile<sup>1</sup>, Cristiana Alberghina<sup>1</sup>, Renata Mangione<sup>3,5</sup>, Joshua D. Bernstock<sup>6</sup>, Cirino Botta<sup>7</sup>, Massimo Gulisano<sup>2,8</sup>, Emanuele Buratti<sup>9</sup>, Giampiero Leanza<sup>10,11</sup>, Robert Zorec<sup>10,11</sup>, Michele Vecchio<sup>12,13</sup>, Michelino Di Rosa<sup>14</sup>, Giovanni Li Volti<sup>3</sup>, Giuseppe Lazzarino<sup>3</sup>, Rosalba Parenti<sup>1,2,15</sup> and Rosario Gulino<sup>1,2,15</sup>

© The Author(s) 2021

Motoneuronal loss is the main feature of amyotrophic lateral sclerosis, although pathogenesis is extremely complex involving both neural and muscle cells. In order to translationally engage the sonic hedgehog pathway, which is a promising target for neural regeneration, recent studies have reported on the neuroprotective effects of clobetasol, an FDA-approved glucocorticoid, able to activate this pathway via smoothened. Herein we sought to examine functional, cellular, and metabolic effects of clobetasol in a neurotoxic mouse model of spinal motoneuronal loss. We found that clobetasol reduces muscle denervation and motor impairments in part by restoring sonic hedgehog signaling and supporting spinal plasticity. These effects were coupled with reduced pro-inflammatory microglia and reactive astrogliosis, reduced muscle atrophy, and support of mitochondrial integrity and metabolism. Our results suggest that clobetasol stimulates a series of compensatory processes and therefore represents a translational approach for intractable denervating and neurodegenerative disorders.

*Cell Death and Disease* (2021)12:625; <https://doi.org/10.1038/s41419-021-03907-1>

## INTRODUCTION

Amyotrophic lateral sclerosis (ALS) is a progressive neurodegenerative disease that affects both upper and lower motoneurons (MNs) [1]. While relatively rare with an incidence of ~2 per 100,000, the clinical course is severe and prognosis dismal with the vast majority of patients dying from respiratory failure 2–5 years after diagnosis [2]. Despite extensive basic and clinical research efforts, the causes of the disease remain to be fully elucidated and no truly effective therapies are yet available [3, 4]. Therefore, the use of animal models appropriately designed to recapitulate the pathology represents a valuable tool for defining new therapeutic approaches [5].

Several data on the pathogenesis of ALS have defined a focal origin in the central nervous system (CNS), where multiple factors contribute to creating a toxic milieu [6, 7], but an active role of both muscle cells and axon terminals in causing retrograde degeneration of MNs has been also proposed as a triggering mechanism [8–10]. Consistently, during the early stages of ALS progression, muscle undergoes denervation, and the gold standard for ALS diagnosis

remains based on nerve conduction analysis and electromyography (EMG) [11]. In our view, the use of reductionist in vivo models would help in the step-by-step dissection of ALS pathogenesis. To this regard, the focal removal of confined populations of spinal MNs by injection of cholera toxin-B conjugated to saporin (CTB-Sap), has proven to be useful in mimicking respiratory dysfunction [12], dysphagia [13], and focal MN loss [14, 15]. It is also worth noting that although MN loss is certainly a critical hallmark of ALS, glial and muscle cells are also involved [16, 17]. Neuroinflammation in ALS has been reported to disrupt homeostatic neuroglial interactions [1]. Moreover, the onset of the disease is known to begin after degeneration is already severe, because plastic mechanisms can compensate for the initial MN loss [18].

Several studies reported that sonic hedgehog (SHH) may represent a crucial regulator of neuroinflammation, neuroprotection, and plasticity [19–22]. SHH serves as a morphogen controlling neural tube patterning during development [23], and also self-renewal and differentiation of neural precursor cells within the postnatal brain

<sup>1</sup>Department of Biomedical and Biotechnological Sciences, Section of Physiology, University of Catania, 95123 Catania, Italy. <sup>2</sup>Molecular Preclinical and Translational Imaging Research Centre - IMPRonTE, University of Catania, 95125 Catania, Italy. <sup>3</sup>Department of Biomedical and Biotechnological Sciences, Section of Biochemistry, University of Catania, 95123 Catania, Italy. <sup>4</sup>Department of Medical, Surgical Sciences and Advanced Technologies G.F. Ingrassia, University of Catania, 95123 Catania, Italy. <sup>5</sup>Department of Basic Biotechnological Sciences, Intensive and Perioperative Clinics, Catholic University of Rome, 00168 Rome, Italy. <sup>6</sup>Department of Neurosurgery, Brigham and Women's Hospital, Harvard University, Boston, MA 02155, USA. <sup>7</sup>Hematology Unit, Annunziata Hospital, 87100 Cosenza, Italy. <sup>8</sup>Department of Drug and Health Sciences, University of Catania, 95123 Catania, Italy. <sup>9</sup>International Centre for Genetic Engineering and Biotechnology (ICGEB), 34149 Trieste, Italy. <sup>10</sup>Laboratory of Cell Engineering, Celica Biomedical, 1000 Ljubljana, Slovenia. <sup>11</sup>Laboratory of Neuroendocrinology – Molecular Cell Physiology, Institute of Pathophysiology, Faculty of Medicine, University of Ljubljana, 1000 Ljubljana, Slovenia. <sup>12</sup>Rehabilitation Unit, AOU Policlinico G. Rodolico, 95123 Catania, Italy. <sup>13</sup>Department of Biomedical and Biotechnological Sciences, Section of Pharmacology, University of Catania, 95123 Catania, Italy. <sup>14</sup>Department of Biomedical and Biotechnological Sciences, Section of Anatomy, Histology and Movement Sciences, University of Catania, 95123 Catania, Italy. <sup>15</sup>These authors contributed equally: Nunzio Vicario, Federica M. Spitale, Daniele Tibullo. Edited by M. Agostini <sup>✉</sup>email: [nunzio.vicario@unicat.it](mailto:nunzio.vicario@unicat.it); [parenti@unicat.it](mailto:parenti@unicat.it); [rogulino@unicat.it](mailto:rogulino@unicat.it)

Received: 17 May 2021 Revised: 4 June 2021 Accepted: 7 June 2021  
Published online: 16 June 2021

[24]. The secreted SHH ligand binds to its receptor Patched, thereby activating smoothened (SMO); this ultimately leads to the nuclear translocation of transcription factors Gli1–3, inducing the expression of target genes [25]. Interestingly, SHH signaling has been shown to play a role in ALS pathogenesis. In particular, the reduction of Gli1 has been reported within the MNs of SOD1<sup>G93A</sup> mice and SHH has been shown to be cytoprotective in vitro [20]. Accordingly, cerebrospinal fluid collected from ALS patients may actually inhibit SHH signaling in vitro [26]. Therefore, SHH signaling represents a druggable target in neurodegenerative disorders [27]. In particular, small molecules targeting SMO have recently been explored in cancer (i.e., SMO antagonists), stroke, and demyelinating disorders (i.e., SMO agonists) [28, 29]. The glucocorticoid clobetasol, which also acts as a SMO agonist, has received attention as a potential therapeutic agent capable of remyelination and neuroprotection/repair [30–32]. However, few data are available regarding the potential effects of SMO activation in MN disease. Therefore, herein we sought to examine the effects of clobetasol treatment in a murine CTB-Sap model of MN degeneration.

## RESULTS

### Clobetasol promotes behavioral improvement by inducing muscle reinnervation

We induced a spinal MN depletion by injecting CTB-Sap toxin into the left gastrocnemius muscle (GM) and assessed the impact of clobetasol treatment on postural and motor performance, as compared to vehicle-treated CTB-Sap-injected mice. Clinical score assessment showed that all animals had a rapid worsening of the left hindlimb postural and motor ability during the first week after lesion (Fig. 1a). Then, clobetasol-treated animals started to ameliorate their clinical score at 14–21 days post lesion (dpl), and this condition was retained up to 42 dpl, whereas vehicle-treated lesioned animals did not ameliorate spontaneously (Fig. 1a). An open field grid walk test was performed in order to evaluate the motor coordination, finding that MN ablation did not affect the distance covered by mice during the grid walk performance (Fig. 1b), but it significantly increased the number of footfalls at 7 dpl as compared to healthy control (HC) group (Fig. 1b). Notably, clobetasol reverted this impairment, promoting a significant reduction of the number of footfalls at 21 and 42 dpl, as compared to vehicle-treated lesioned mice (Fig. 1b).

EMG recordings from the left GM showed typical clinical evidence of denervation, such as positive sharp waves (PSW), fibrillation (Fig. 1c, d), pseudo-neuromyotonia (NMT, Fig. 1c–e), and fasciculations (Fig. 1c–f). Notably, clobetasol-treated CTB-Sap-lesioned mice showed a significant 70% reduction of PSW and fibrillation compared to the vehicle-treated group (Fig. 1c). This evidence was coupled with a reduced number and size of AChE-positive spots in the left GM and a near-normal pattern in clobetasol-treated mice (Fig. 1g). Together, these data suggest that clobetasol exerts restorative behavioral effects and promotes muscle reinnervation after neurotoxic MN removal.

### Clobetasol promotes spinal cord plasticity acting on SHH signaling pathway

Neuropathological assessment of lumbar spinal cord sections revealed a depletion of about 50% of MNs in the lesioned (i.e. left) side compared to the intact spinal cord side (Fig. 2a–c), and this rate of MN loss was present in all CTB-Sap-lesioned mice, regardless of the drug treatments. This suggests that the functional amelioration and muscle reinnervation is linked to compensatory plastic changes within the spared MN population.

In order to link our observations with a potential activation of the SHH signaling pathway in the spinal cord, we analyzed Gli1 nuclear translocation in resident cell populations of HC and CTB-Sap mice treated with either vehicle or clobetasol. Results showed that the total fluorescence intensity (FI) of Gli1 was unchanged (Fig. 2d),

whereas a significant reduction of nuclear Gli1 FI was found in CTB-Sap-lesioned mice at 42 dpl, but near-normal levels were found in CTB-Sap mice treated with clobetasol (Fig. 2e). To analyze such a modulation into specific cell populations, we evaluated the Gli1 nuclear translocation in NeuN (i.e. neurons), Gfap (i.e. astrocytes), and Iba1 (i.e. microglia) positive cells. Our data highlighted that clobetasol was able to significantly increase the amount of nuclear Gli1 in NeuN-positive cells by about 2 folds (Fig. 2f, g). Moreover, a reduction of nuclear Gli1 was found in the astroglial cell population after lesion but, importantly, near-normal levels were present in clobetasol-treated mice (Fig. 2f–h). Finally, neither CTB-Sap lesion nor clobetasol treatment did affect nuclear translocation of Gli1 in microglia (Fig. 2f–i). We also analyzed the potential effect of clobetasol in modulating spinal MN plasticity. Lesioned animals treated with clobetasol showed a remarkable increase of newly formed synaptic contacts labeled with synaptophysin, as compared to both vehicle-treated lesioned mice and HC (Fig. 2j).

### Clobetasol modulates metabolic changes in MN-depleted spinal cord

We examined the metabolic profiles of the intact and lesioned spinal cord either with or without clobetasol treatment (Figs. S1 and S2). Our results suggest that amino acids biosynthesis metabolic pathways (Fig. 3a–c), lysine, tryptophan, and arginine levels were significantly modulated in CTB-Sap clobetasol versus CTB-Sap vehicle mice (Fig. 3d). We also observed that isoleucine levels were slightly, but not significantly, reduced in CTB-Sap vehicle group and significantly decreased in CTB-Sap clobetasol mice (Fig. 3d). Among the highest contributors to the PCA analysis (Fig. S2) we found that hypoxanthine and xanthine were of importance and they were significantly higher in CTB-Sap vehicle mice (Fig. 3d), while clobetasol reverted such accumulation to the level of healthy spinal tissue (Fig. 3d). Results also revealed that CTB-Sap lesion was associated with a reduction of GABA and glycine, both involved in spinal inhibitory circuitry and that clobetasol was able to restore near-normal levels of both neurotransmitters (Fig. 3d). Interestingly, even in presence of a reduced number of MNs in the lesioned spinal cord side (about 50%), no significant changes were observed in glutamate levels (Fig. 3d), thus suggesting that spared MNs could probably receive increased glutamate signaling as compared to HC MNs.

### Clobetasol reduces pro-inflammatory resident cells in MN-depleted spinal cord

MN ablation was associated with an increased total number of Gfap<sup>+</sup> astrocytes in the Rexed lamina IX of CTB-Sap-lesioned mice treated with vehicle, whereas clobetasol-treated group showed an apparent but not statistically significant increase over control levels (Fig. 4a, b). However, the total Gfap mRNA levels measured in the spinal cord were similar in both lesioned groups, with a significant increase above control levels (Fig. 4c). In order to clarify whether spinal astrocytes were polarized towards a reactive state, we analyzed phospho-stat-3 (P-Stat3) expression in spinal Gfap<sup>+</sup> cells (Fig. 4d). Our evidence supports the hypothesis that MN depletion increases the number of reactive astrocytes, and that clobetasol was able to reduce nuclear P-Stat3 expression in lamina IX, thus partially reversing the effects of the lesion.

We also performed a multidimensional flow cytometry analysis of spinal cord samples to characterize the myeloid compartment (i.e. tissue-resident microglia phenotypes, monocytes, monocytes-derived macrophages) and, due to shared markers, also B and non-B (i.e. T NK) lymphocytes (Fig. S3). Interestingly, our results showed that MN depletion increased the frequency of CD206<sup>+</sup> and CD80<sup>+</sup> inflammatory microglia and that clobetasol, besides reducing polarized microglial cells (Fig. 4e, f), also reduced the total amount of B and T NK lymphocytes (Fig. 4e, f). These findings suggest that clobetasol was able to attenuate the pro-inflammatory signaling in the spinal cord, thus likely promoting plasticity and compensatory processes.

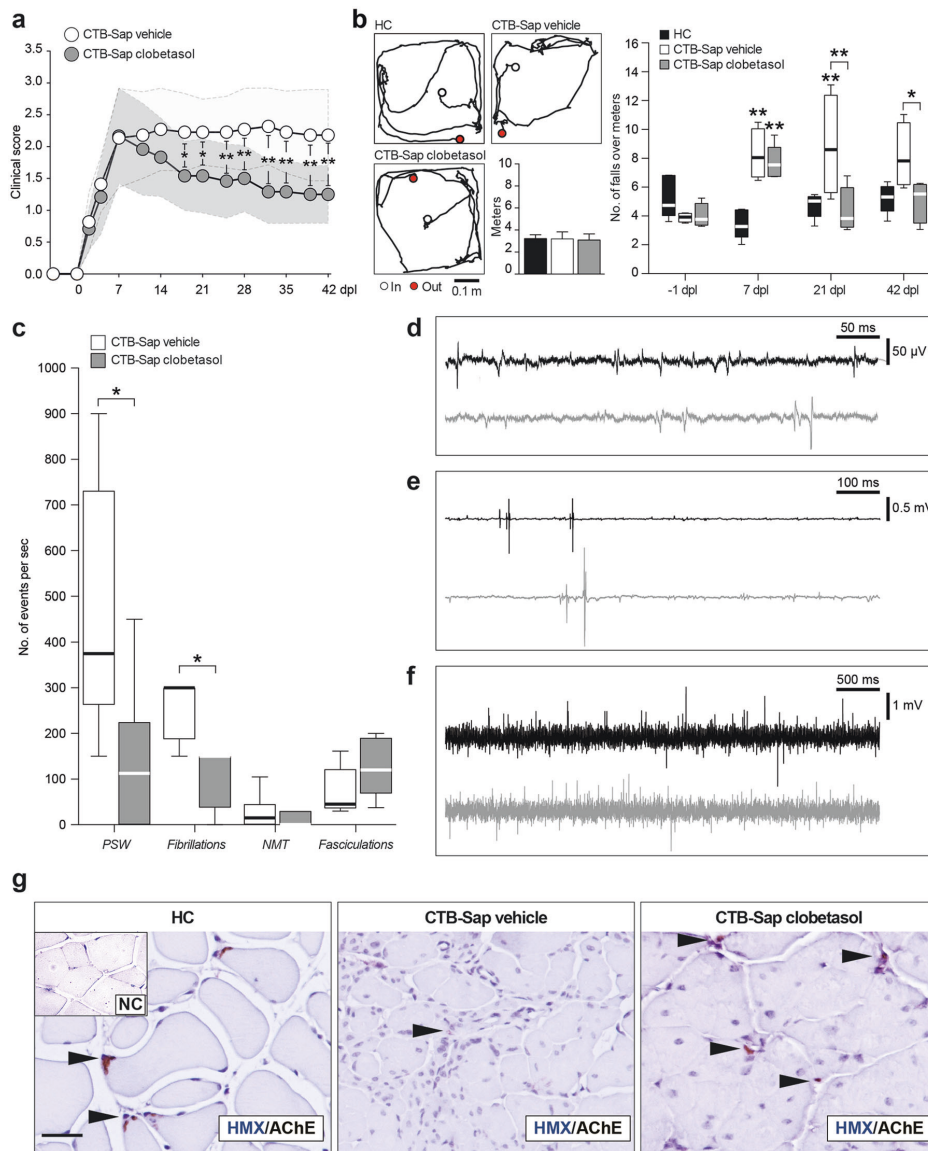


**Fig. 1** Clobetasol ameliorates behavioral impairment of CTB-Sap-induced MN ablation. **a** Repeated measures of a clinical score of motor impairment during the time-course of CTB-Sap-induced motoneuronal depletion in CTB-Sap vehicle and CTB-Sap clobetasol groups; data are shown as mean  $\pm$  SEM of  $n = 12$  mice per group; \* $p$ -value  $< 0.05$  and \*\* $p$ -value  $< 0.01$  between groups; two-way repeated-measures ANOVA. **b** Representative tracks of HC, CTB-Sap vehicle, and CTB-Sap clobetasol groups and quantification of the distance (expressed as mean meters  $\pm$  SEM of  $n = 5$  mice per time-point, as repeated measures) covered during 2 min performance on open-field grid walk test and quantification of the number of footfalls over a meter at  $-1$ , 7, 21 and 41 dpi in HC, CTB-Sap vehicle, and CTB-Sap clobetasol groups; data are shown as standard box-and-whiskers of  $n = 5$  mice per group; \* $p$ -value  $< 0.05$  and \*\* $p$ -value  $< 0.01$  versus HC and between groups; two-way repeated-measures ANOVA. **c–f** Quantification and representative electromyographic profile of positive sharp waves (PSW, **c** and **d**), fibrillations (**c** and **e**), pseudo-neuromyotonia (NMT, **c** and **e**), and fasciculations (**c** and **f**) observed in denervated GM in CTB-Sap vehicle (black tracks in **d–f**) and CTB-Sap clobetasol groups (gray tracks in **d–f**); data are expressed as a number of events per second and showed as standard box-and-whiskers of  $n = 4$  mice per group; measures were taken from distinct samples; \* $p$ -value  $< 0.05$  versus CTB-Sap vehicle; two-sided Student's  $t$ -test. **g** Representative pictures of AChE immunostaining and hematoxylin (HMX) and negative control (NC) on left GM of HC, CTB-Sap vehicle, and CTB-Sap clobetasol; scale bar: 25  $\mu$ m. Dpl: days post lesion.



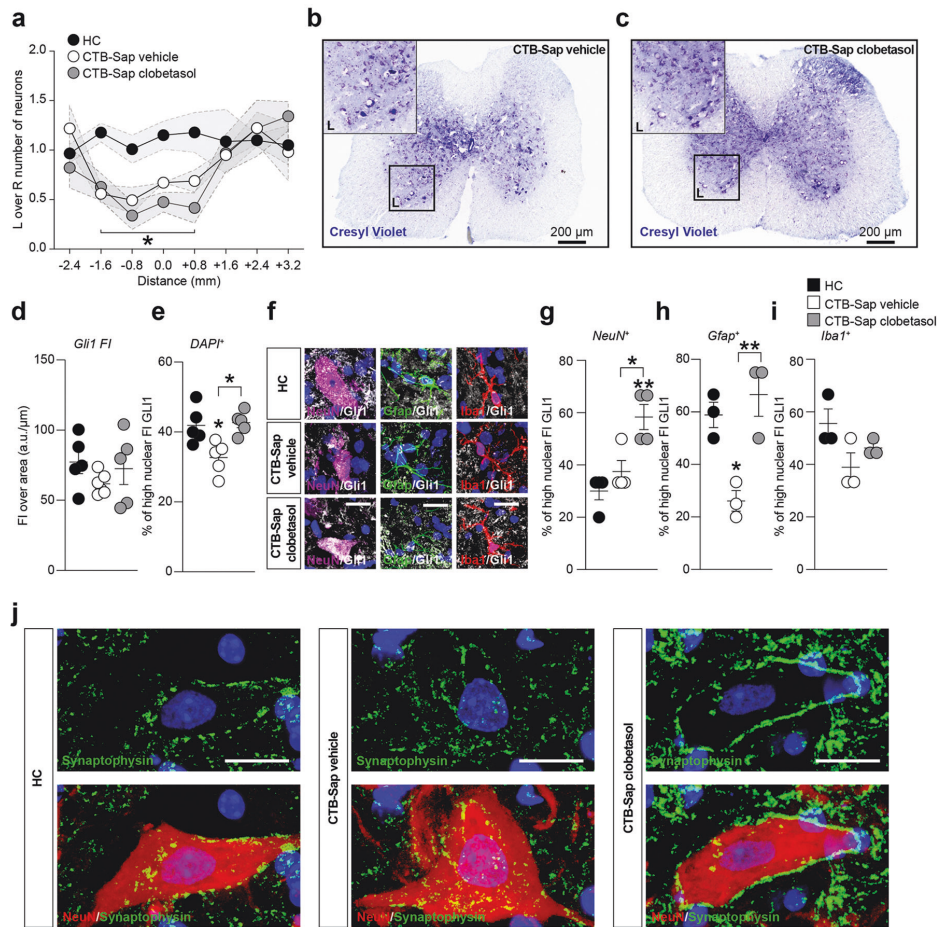


**Fig. 2 Clobetasol modulates Gli1 nuclear translocation and plasticity on MN-depleted spinal cord.** **a–c** Quantification of the number of motoneurons in left (L) and right (R) Rexed lamina IX in HC, CTB-Sap vehicle and CTB-Sap clobetasol groups (**a**) and representative pictures of spinal cord sections stained with cresyl violet of CTB-Sap vehicle (**b**) and CTB-Sap clobetasol (**c**); data in (**a**) are expressed as the ratio of L over R motoneurons number  $\pm$  SEM (shade) of  $n = 8$  sections of  $n = 5$  mice per group; \* $p$ -value  $< 0.05$  versus HC; one-way ANOVA; scale bar in (**b**) and (**c**); 200  $\mu$ m. **d** and **e** Quantification of the total Gli1 fluorescence intensity (FI) over  $\mu$ m (**d**) and of the percentage of high nuclear FI of Gli1 (**e**) in HC, CTB-Sap vehicle, and CTB-Sap clobetasol spinal cord cell population; data are shown as scatter dot plots and mean  $\pm$  SEM of  $n \geq 3$  mice per group; \* $p$ -value  $< 0.05$  versus HC and between groups; one-way ANOVA. **f–i** Representative pictures and quantification of the proportion of NeuN positive (**f** and **g**), Gfap positive (**f** and **h**), and Iba1 positive (**f** and **i**) cells with high nuclear FI of Gli1 in HC, CTB-Sap vehicle, and CTB-Sap clobetasol spinal cord; data are shown as scatter dot plots and mean  $\pm$  SEM of  $n \geq 3$  mice per group; \* $p$ -value  $< 0.05$  and \*\* $p$ -value  $< 0.01$  versus HC and between groups; one-way ANOVA. **j** Representative pictures of NeuN and Synaptophysin immunofluorescence on spinal cord motoneurons of HC, CTB-Sap vehicle, and CTB-Sap clobetasol; scale bar: 20  $\mu$ m.

**Clobetasol promotes trophic processes in the denervated muscle**

In order to associate the CNS effects induced by clobetasol with the observed functional restoration, we analyzed the morphological and metabolic changes of muscles. Our data indicate that, after the partial denervation caused by MN removal, muscle fibers in GM showed an increased number of centrally located nuclei (CLN) as compared to HC (Fig. 5a, b), but clobetasol treatment significantly reduced the proportion of myofibers with CLN (Fig. 5b). To assess muscle atrophy, we evaluated the cross-sectional area of myofibers in GM of CTB-Sap mice treated with vehicle or clobetasol, finding an overall increase of fiber area in clobetasol-treated mice compared to vehicle-treated, even if it did not reach the physiological pattern found in HC mice

(Fig. 5a–c). Such an amelioration was coupled with increased Pax7<sup>+</sup> cells in GM of clobetasol-treated mice (Fig. 5d). Furthermore, we found a significantly increased amount of F4/80<sup>+</sup> infiltrating macrophages in both vehicle-treated and clobetasol-treated denervated muscles (Fig. 5e, f). To determine the phenotype of infiltrating macrophages in GM of vehicle-treated and clobetasol-treated mice, we analyzed F4/80<sup>+</sup> cell phenotype (Fig. 5g) by quantifying those highly expressing iNos or Arg1. The results revealed that clobetasol was able to significantly increase the proportion of anti-inflammatory infiltrating macrophages into denervated GM (Fig. 5g, h), thus likely sustaining a pro-regenerative microenvironment. Finally, we analyzed the metabolic effects induced by denervation onto GMs (Fig. S4–S6). PCA analysis revealed that inosine monophosphate (IMP),

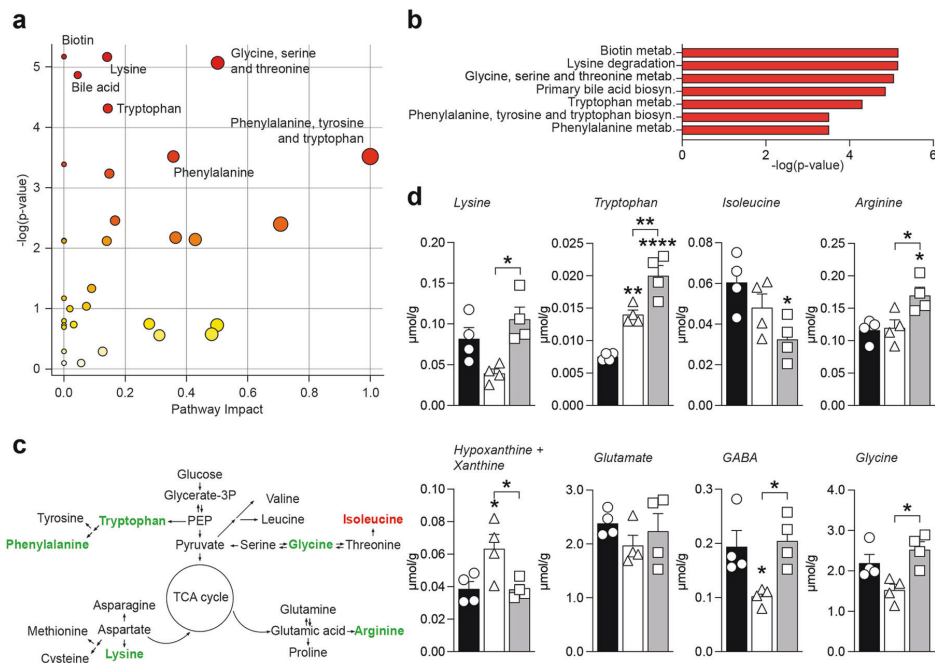


**Fig. 3** Clobetasol modifies spinal cord metabolism and relevant neurotransmitters. **a** and **b** Summary plot for pathway analysis (**a**) and quantitative enrichment analysis (**b**) for metabolites levels in CTB-Sap vehicle versus CTB-Sap clobetasol; **c** Schematic representation of amino acids biosynthesis showing significantly upregulated (green) and downregulated (red) metabolites in CTB-Sap clobetasol versus CTB-Sap vehicle group. **d** Metabolites levels in the spinal cord of HC, CTB-Sap vehicle and CTB-Sap clobetasol mice; data are shown as mean  $\pm$  SEM and scattered dot plots of  $n = 4$  mice per group; \* $p$ -value  $< 0.05$ , \*\* $p$ -value  $< 0.01$ , \*\*\*\* $p$ -value  $< 0.0001$  versus HC or between groups; one-way ANOVA.

hypoxanthine, xanthine, and uric acid played a major role. This analysis also highlighted that purine nucleotide catabolism and fatty acid biosynthesis and elongation were strictly regulated in denervated GM (Fig. 5i). We observed a robust accumulation of IMP, hypoxanthine, xanthine, and uric acid in CTB-Sap vehicle group (Fig. 5j, k), which suggests an overproduction of reactive oxygen species in the muscular microenvironment, and a decreased availability of malonil-CoA for fatty acid biosynthesis (Fig. 5j). Such evidence suggests that denervation shapes purine and fatty acid metabolism in the muscle and that clobetasol was able to revert this condition (Fig. 5j), promoting favorable metabolic programs after CTB-Sap-induced muscle denervation.

#### Clobetasol reverts denervation-induced mitochondrial fission and increases energy substrates

Mitochondrial morphology was assessed in muscle sections, finding that denervation strongly affected mitochondrial fitness, as shown by the significant reduction of mitochondrial length (Fig. 6a, b) and by the significant increase of dynamin-like 1 (*Dnm1*) mRNA levels, which is an essential gene controlling mitochondrial fission (Fig. 6c). Notably, clobetasol-treated CTB-Sap-lesioned mice showed increased mitochondrial length, coupled with a normalization of *Dnm1* mRNA levels (Fig. 6a–c), suggesting a restored mitochondrial homeostasis and energy metabolism in clobetasol-treated mice. Then, we analyzed phosphate nucleotides, nicotinic coenzymes, and glycosylated UDP-derivatives (Fig. 6d and Fig. S7). The results highlighted a significant accumulation of glycosylated UDP-derivatives and monophosphate nucleotides coupled with a reduction of ATP in GM of CTB-Sap mice treated with vehicle (Fig. 6e), and these effects were reverted by clobetasol (Fig. 6f). Indeed,

UDP-Gal, UDP-GalNac, UDP-Glc, and UDP-GlcNac (Fig. 6g), were all significantly increased in CTB-Sap-vehicle mice, whereas clobetasol treatment induced their normalization (Fig. 6g).

Notably, by measuring the levels of nicotinic coenzymes, we found a strong decrease of the oxidized over reduced form of NAD and NADP, thus indicating a reduced mitochondrial redox potential in denervated GM as compared to HC and clobetasol-treated lesioned group (Fig. 6g). Finally, we evaluated the ratio between ATP and ADP and the energy charge potential (ECP). Our data highlighted an overall increase of ATP/ADP ratio and ECP induced by clobetasol versus vehicle group (Fig. 6g), thus supporting the hypothesis of restored energy metabolism.

#### Human ALS spinal cord shows impaired SHH signaling pathway

In order to evaluate the potential involvement of SHH signaling pathway in human ALS patients, we first performed a z-score analysis of a selected dataset containing mRNA expression data from spinal cord biopsies of  $n = 10$  HC subjects and  $n = 10$  ALS patients. Despite similar *SHH* mRNA expression levels (Fig. 7a), we found a significant reduction of *PTCH1* mRNA levels in the spinal cord of ALS patients (Fig. 7b). Notably, this reduction was not coupled with a reduction of *SMO* mRNA levels (Fig. 7c), but it was coupled with reduced mRNA levels of SHH-signaling pathway effector *GLI1* (Fig. 7d). This would suggest that SHH signaling pathway may represent a promising target for pharmacological treatment of MN diseases using SMO agonists.

Moreover, the interaction network of SHH signaling pathway genes *SHH*, *PTCH1*, *SMO*, *GLI1*, *GLI2*, and *GLI3* showed significant interactions, based on available databases or experimentally

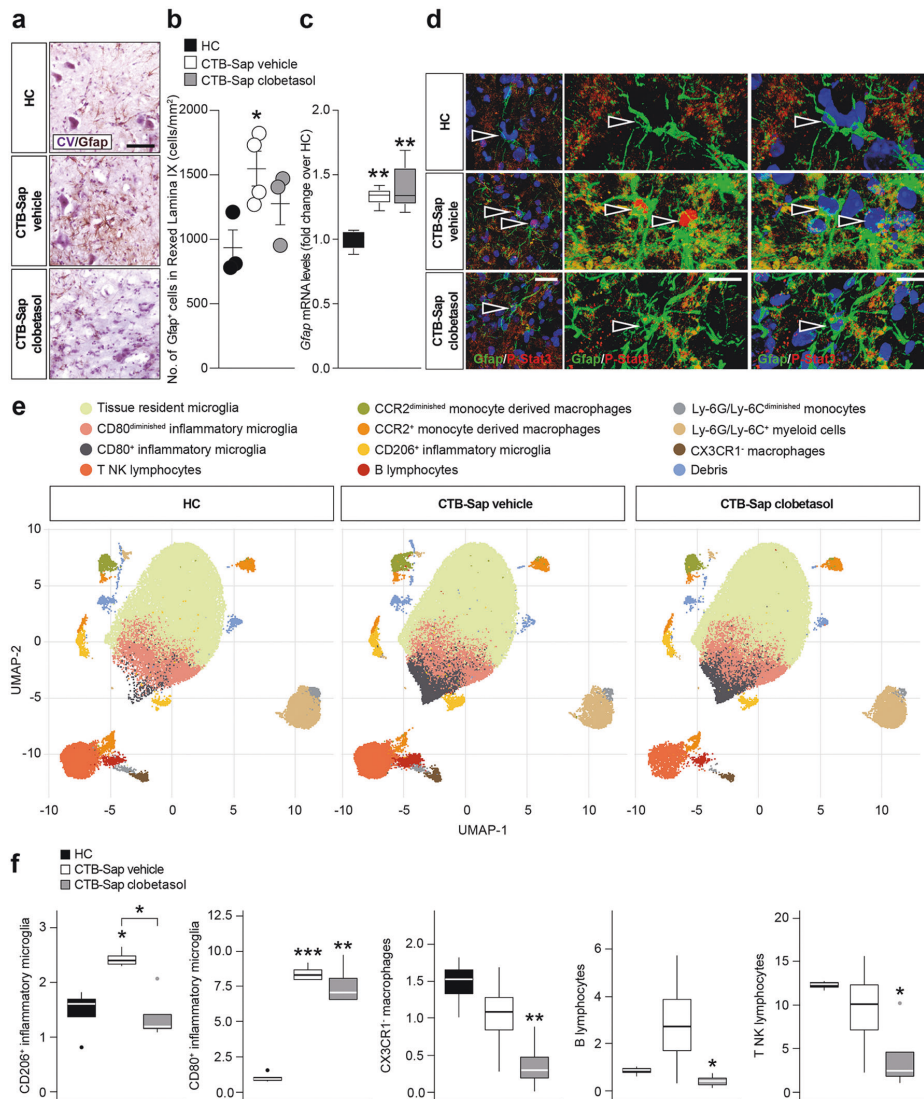
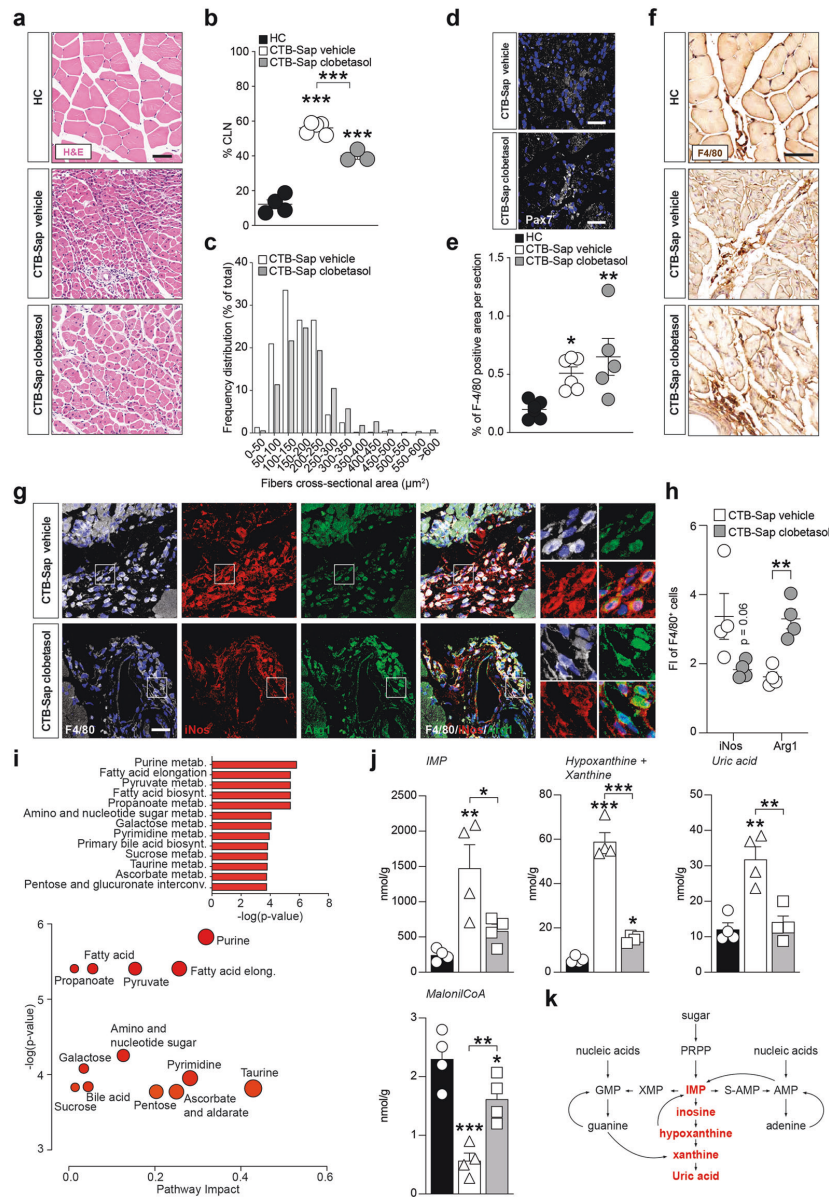


**Fig. 4 Clobetasol-mediated reduction of pro-inflammatory cells in MN-depleted spinal cord.** **a** and **b** Representative pictures of Gfap immunostaining (**a**) and quantification of the number of positive cells for Gfap (**b**) in HC, CTB-Sap vehicle, and CTB-Sap clobetasol spinal cord; data are shown as scatter dot plot and mean  $\pm$  SEM of  $n \geq 3$  mice per group; \* $p$ -value < 0.05 versus HC; one-way ANOVA; scale bar in (**a**): 25  $\mu$ m. **c** mRNA levels of Gfap in the spinal cord of in HC, CTB-Sap vehicle, and CTB-Sap clobetasol spinal cord; data are shown as standard box-and-whiskers plot and mean  $\pm$  SEM of  $n \geq 3$  mice per group; \*\* $p$ -value < 0.01 versus HC; one-way ANOVA. **d** Representative pictures and confocal deconvolutions of Gfap and P-Stat3 staining in HC, CTB-Sap vehicle, and CTB-Sap clobetasol spinal cord; arrowheads indicate astrocytes nuclei and in CTB-Sap vehicle P-Stat3 positive nuclei; scale bar: 20  $\mu$ m. **e** Uniform manifold approximation and projection (UMAP) representation of the populations identified through flow-cytometry in the three different conditions. **f** Standard box-and-whiskers plot representing the five subpopulations that presented a significant modulation between HC, CTB-Sap vehicle, and CTB-Sap clobetasol mice. Plots show data from  $n = 4$  mice per group; \* $p$ -value < 0.05 versus CTB-Sap vehicle; one-way ANOVA.

determined in humans, between the six selected genes (i.e. query) and the top-20 interactor genes (Fig. 7e). Enrichment KEGG analysis revealed significant modulation of pathways involved in chemokine signaling, axon guidance, synapses, and neurotransmission (Fig. 7f), thus supporting the idea that SHH modulation holds great relevance in human CNS homeostasis and compensatory processes.

**DISCUSSION**

Several studies have shown that alterations of spinal cord circuitries and MNs can start far earlier than the onset of symptoms [33, 34]. This suggests that compensatory changes occur in an attempt to maintain neuromuscular functions despite the progressive loss of motor units, and the possibility to target this plasticity coupled with



efficient methods of early diagnosis would increase the chances of delaying the disease progression and hopefully promoting repair. Although genetic mouse models of ALS are necessary to model the human disease, reductionist animal models, such as the CTB-Sap model, are useful to dissect specific pathogenic mechanisms, since they are able to mimic a limited and controlled series of disease features. In our CTB-Sap model of spinal MN removal, the severity of the lesion and, as a consequence, the capability of self-restoration, can be modulated simply by choosing different doses of CTB-Sap. After administration of relatively low doses of toxin, mice were able

to recover as soon as 4–6 weeks after the lesion [15]. Increased activity in the spared MNs and surrounding circuitries, likely driven by synaptic plasticity, could be responsible for these compensatory changes with possible involvement of SHH [35, 36].

In the present study, in order to test the effects of modulating the SHH pathway by the SMO agonist clobetasol, we used a dose of CTB-Sap able to ablate about 50% of resident MNs, and inducing a stable motor impairment, without any spontaneous amelioration up to 6 weeks post-lesion. The effects of clobetasol treatment were then evaluated from functional, metabolic, and pathophysiological

**Fig. 5 Clobetasol increases muscle fiber size and metabolism.** **a** Representative pictures of H&E staining in left GM of HC, CTB-Sap vehicle, and CTB-Sap clobetasol mice; scale bar: 25  $\mu$ m. **b** Quantification of the percentage of centrally located nuclei (CLN) in HC, CTB-Sap, and CTB-Sap clobetasol-treated mice; data are % of CLN over total muscle fibers and are shown as scatter dot plot and mean  $\pm$  SEM of  $n \geq 3$  mice per group; \*\*\* $p$ -value < 0.001 versus HC or between groups; one-way ANOVA. **c** Frequency plot of the mean fiber cross-sectional area expressed in  $\mu$ m<sup>2</sup> in the left GM of CTB-Sap vehicle and CTB-Sap clobetasol mice. **d** Representative pictures of Pax7 positive cells in the left GM of CTB-Sap vehicle and CTB-Sap clobetasol mice. **e** and **f** Quantification of the percentage of F4/80 positive area per section (**e**) and representative pictures of F4/80 immunostaining (**f**) in the left GM of HC, CTB-Sap vehicle, and CTB-Sap clobetasol mice; data in (**e**) are shown as scatter dot plot and mean  $\pm$  SEM of  $n \geq 3$  mice per group; \* $p$ -value < 0.05 and \*\* $p$ -value < 0.01 versus HC; one-way ANOVA; scale bar in (**f**): 25  $\mu$ m. **g** and **h** Representative pictures of F4/80, iNos and Arg1 immunostaining (**g**) and quantification of the FI of iNOS and Arg1 in F4/80 positive cells (**h**) in the left GM of CTB-Sap vehicle and CTB-Sap clobetasol mice; data in (**h**) are shown as scatter dot plot and mean  $\pm$  SEM of  $n \geq 3$  mice per group; \*\* $p$ -value < 0.01 versus CTB-Sap vehicle; two-sided Student's  $t$ -test. Scale bar in (**g**): 25  $\mu$ m. **i** Summary plot for quantitative enrichment analysis and pathway analysis for metabolites levels in CTB-Sap vehicle versus CTB-Sap clobetasol; **j** Metabolites levels in the left GMs of HC, CTB-Sap vehicle, and CTB-Sap clobetasol mice; data are shown as mean  $\pm$  SEM and scattered dots plot of  $n = 4$  mice per group; \* $p$ -value < 0.05 and \*\* $p$ -value < 0.01 versus HC or between groups; one-way ANOVA. **k** Schematic representation of purine metabolism showing significantly upregulated metabolites in red in CTB-Sap vehicle versus CTB-Sap clobetasol group.

aspects. After CTB-Sap injection, animals developed a rapid motor impairment of the affected hindlimb during the first week and these deficits appeared very stable during the entire experimental time-course in vehicle-treated animals. Interestingly, when animals were treated with clobetasol, a significant improvement of behavioral signs was observed as early as 3 weeks post-lesion and animals became able to near-normal walking.

These effects were coupled with reduced muscle denervation in clobetasol-treated mice. The post-mortem analysis of the spinal cord revealed a down-regulation of synaptophysin expression by the spared lumbar MNs, suggesting a decreased number of synapses on their somata after removal of neighboring MNs. Interestingly, lesioned animals treated with clobetasol showed an increased expression of synaptophysin, which is supposed to be linked to MN plasticity and functional restoration. Accordingly, the quantitative analysis of spinal cord metabolites has revealed a decrease of the inhibitory neurotransmitters GABA and glycine in lesioned animals. Moreover, although the level of glutamate was unchanged in the lumbar spinal cord after the lesion, we should consider that it acts onto a reduced population of MNs. Taken together, these findings suggest an attempt of spinal cord circuitries to compensate for the decreased neuromuscular activity, and the restoration of GABA and glycine levels after clobetasol treatment can suggest a rebalancing of neuronal activity promoted by the drug. Other critical aminoacids were affected by both MN removal and SMO modulation. Among them, we found significant alterations of lysine, tryptophan, arginine, and isoleucine, suggesting profound metabolic changes in the lesioned and treated spinal cord, involving glycolysis and tricarboxylic acid cycle. These changes are also present in patients, as well as in ALS experimental models [37, 38].

Our observation of astrocytes and microglial modulation is in line with increased levels of hypoxanthine and xanthine, the conversion of which produces a significant accumulation of reactive oxygen species. This could represent a major cause of neuronal suffering and it is also the rationale for edaravone treatment of ALS patients [39]. Notably, our results demonstrate that clobetasol is also able to reduce immune response not only modulating astrocytes and microglia polarization but also attenuating B and T NK lymphocyte infiltration.

The analysis of muscle also showed profound changes after CTB-Sap-induced denervation and as a result of treatment with clobetasol. Denervated GMs appeared atrophic but, interestingly, a five-fold increase of the number of CLN was detected in muscle sections, thus suggesting an attempt of regeneration [40]. The regenerative potential of the denervated muscle was boosted by administration of clobetasol, as demonstrated by the increased expression of Pax7 and by the increased cross-sectional area of muscle fibers, together with the reduction of CLN in comparison to the lesioned and vehicle-treated muscle. Taken together, the observed changes of GM morphology indicate that clobetasol may accelerate the muscle repairing processes.

The effect of CTB-Sap injection on muscle metabolism was observed in most of the metabolites under evaluation. A dramatic decrease in the ATP/ADP ratio, ECP, NAD<sup>+</sup>/NADH ratio, NADP<sup>+</sup>/NADPH ratio, concomitantly accompanied by an increase in oxypurines (hypoxanthine, xanthine, uric acid), IMP, nitrite, and nitrate, are clear indicators of mitochondrial dysfunction, also suggested by increased mitochondrial fission, with an imbalance in ATP production and consumption, consequent energy stress, the compensatory metabolic shift towards oxygen-independent glucose consumption through glycolysis, and oxidative/nitrosative stress with decreased antioxidant defenses. Among the various alterations of cell metabolism, those occurring to UDP-derivatives are certainly the most evident. The higher values of nucleotide sugars strongly suggest that the hexosamine biosynthetic pathway, representing the key process for the post-translational protein glycosylation, is highly active in damaged muscle. This finding may be indicative either of increased production of myokines or fibro/adipogenic processes, both being also reported as ALS-linked skeletal muscle changes [41, 42].

We hypothesize that clobetasol, acting as a glucocorticoid, could mobilize fatty acids and we found that, in denervated muscle, reduced malonil-CoA levels were present. Indeed, clobetasol was able to revert this phenomenon increasing fatty acid metabolism. Such results are in line with previously published reports linking hypolipidemia and dyslipidemia with ALS progression [43, 44].

Taken together, our data suggest that clobetasol exerts a pleiotropic effect in both the spinal cord and muscle finally resulting in neuromuscular plasticity. We can draw a number of conclusions from these observations. First, MNs depletion is associated with behavioral impairment and substantial neuromuscular alterations ranging from metabolic changes to the activation of immune response in the spinal cord, and from critical myopathy to energetic imbalance in the muscle. Second, the multitarget drug clobetasol acts by increasing Gli1 nuclear translocation in spinal astrocytes and spared MNs, reverting the known canonical SHH reduction that we observed in our experimental model of denervation [14, 36]. Third, robust inhibition of muscular fatty acid metabolism was observed in denervated mice and such a reduction was reverted by clobetasol.

In summary, these results confirm the existence of significant capacity of neuromuscular plasticity, which can be manipulated by drugs affecting a number of targets, including metabolism, reactive neuroglia and CNS infiltrating lymphocytes, synaptic plasticity, and muscle regeneration. Among these targets, particular attention should be paid to the SHH signaling, also in relation to MN diseases. The existence of an already approved drug-like clobetasol acting onto this pathway increases the interest in this promising potential therapeutic approach in ALS.

Interestingly, our work highlighting the role of SHH pathway in human ALS patients, suggests that the described results could be relevant for human ALS. Further studies also including SMO

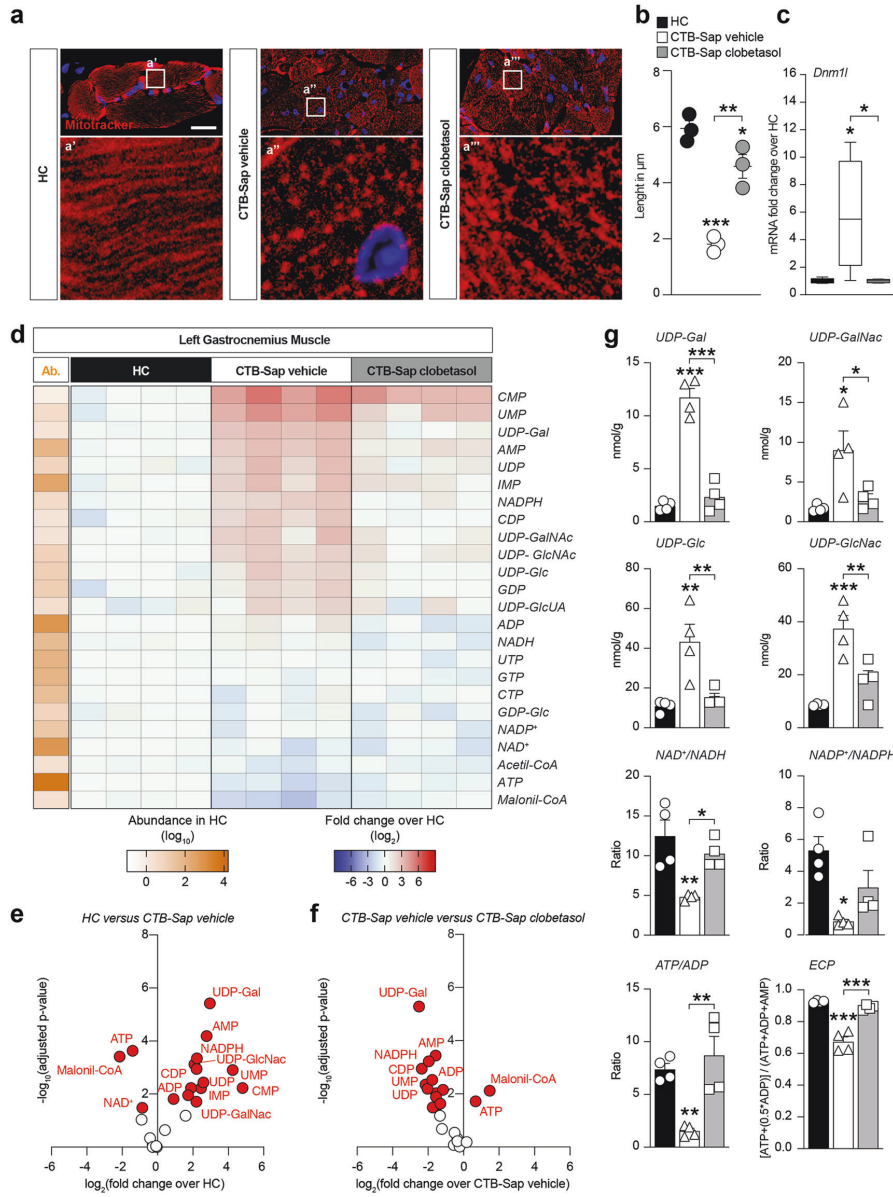


**Fig. 6 Clobetasol reverts denervation-induced mitochondrial fission and increases energy substrates.** **a** and **b** Representative pictures of Mitotracker immunostaining (**a**) and quantification of the mitochondrial length expressed in  $\mu\text{m}$  (**b**) in the left GM of HC, CTB-Sap vehicle, and CTB-Sap clobetasol mice; data in (**b**) are shown as scatter dot plot and mean  $\pm$  SEM of  $n \geq 3$  mice per group; \* $p$ -value  $< 0.05$ , \*\* $p$ -value  $< 0.01$  and \*\*\* $p$ -value  $< 0.001$  versus HC or between groups; one-way ANOVA; scale bar in (**a**):  $25 \mu\text{m}$ . **c** mRNA expression levels of *Dnm1* in the left GM of HC, CTB-Sap vehicle and CTB-Sap clobetasol mice; data are fold changes over HC and are shown as standard box-and-whiskers plot of  $n = 5$  mice per group; \* $p$ -value  $< 0.05$  versus HC or between groups; one-way ANOVA. **d** Heat maps of 24 metabolites in the left GM HC, CTB-Sap vehicle and CTB-Sap clobetasol at 42 dpl showing the abundance (Ab.) in HC and the relative changes in CTB-Sap vehicle and CTB-Sap clobetasol as compared to HC; data are shown as  $\log_{10}$  abundance and  $\log_2$  FC over HC of  $n = 4$  mice per group. **e** and **f** Volcano plots of metabolites levels in HC versus CTB-Sap vehicle (**e**) and CTB-Sap vehicle versus CTB-Sap clobetasol (**f**). **g** Metabolites levels and ratios in the left GMs of HC, CTB-Sap vehicle, and CTB-Sap clobetasol mice; data are shown as mean  $\pm$  SEM and scattered dots plot of  $n = 4$  mice per group; \* $p$ -value  $< 0.05$  and \*\* $p$ -value  $< 0.01$  versus HC or between groups; one-way ANOVA.

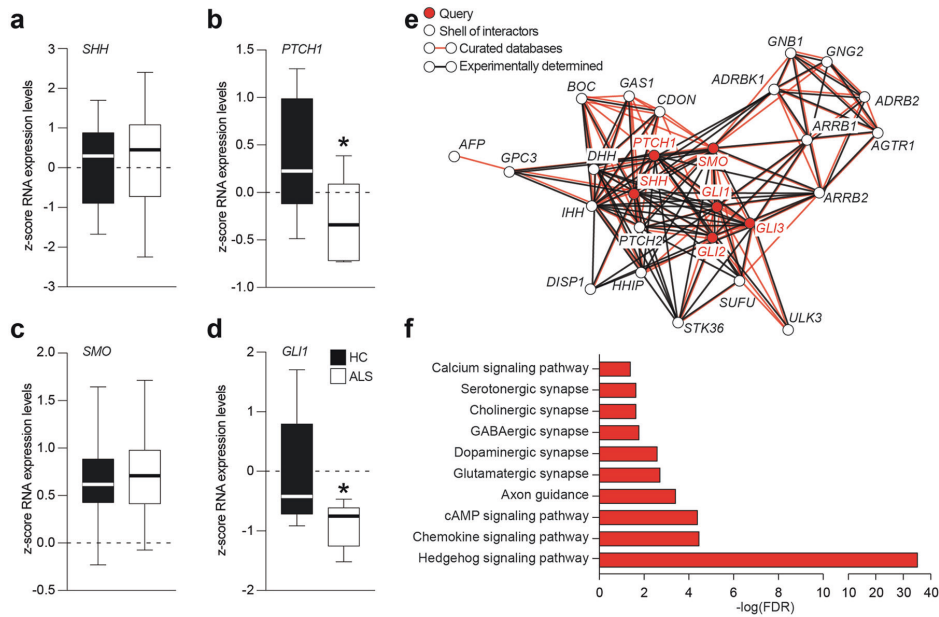


**Fig. 7 SHH signaling pathway is downregulated in ALS.** **a–d** Analysis of SHH (**a**), PTCH1 (**b**), SMO (**c**), and GLI1 (**d**) expression levels in spinal cord biopsies of human healthy control (HC) and ALS patients; data are shown as standard box-and-whiskers of  $n = 10$  HC and  $n = 10$  ALS subjects; \* $p$ -value  $< 0.05$  versus HC; two-sided Student's  $t$ -test. **e** Interaction network of six selected genes (i.e. query) of SHH signaling pathway (in red) and the top-20 interactors genes (in white); interactions are shown as based on curated databases (red lines) or experimentally determined (black lines). **f** Enrichment KEGG analysis of genes showed in panel (**e**); significant pathways related to SHH signaling in humans are shown as  $-\log(\text{FDR})$ .

agonists in other animal models might provide additional evidence about the potential bench-to-bedside translation of the findings described here.

**MATERIALS AND METHODS**

**Animal model**

All experiments were performed in accordance with the principle of the Basel Declaration as well as to the European and Italian regulations (2010/63/EU and Italian D. Lgs. no. 26/2014). All efforts were made to replace, reduce and refine the use of laboratory animals. Moreover, the study was conducted in accordance with the recommendations of the local committee for animal welfare (OPBA, University of Catania, Catania, Italy); the protocol was approved by OPBA and by the Italian Ministry of Health. 48 male 129S1/SvImJ (Jackson Laboratory), 8–12 weeks old and weighing  $25.6 \pm 0.4$  g were used. Animals were randomly assigned to different cages ( $n \leq 5$  animals per cage) and kept under constant temperature ( $23–25^\circ\text{C}$ ) with ad libitum access to food and water. Mice were divided into three groups: HC group (no injection,  $n = 16$ ), CTB-Sap clobetasol (injected with CTB-Sap and then treated with clobetasol propionate,  $n = 16$ ), and CTB-Sap vehicle group (injected with CTB-Sap and then treated with drug vehicle only,  $n = 16$ ). CTB-Sap injection was performed as previously described [45, 46]. Briefly, mice were anesthetized with isoflurane (4% for induction, 2% for maintenance) and then received two injections of the ribosome-inactivating and retrogradely transported toxin CTB-Sap (Advanced Targeting Systems, San Diego, CA, USA) into the medial and lateral left gastrocnemius with a toxin dose of  $6 \mu\text{g}/2 \mu\text{L}$  in PBS per injection. Subgroups of CTB-Sap lesioned mice received an intraperitoneal injection of either clobetasol propionate ( $4 \text{ mg}/\text{kg}$ ) or vehicle alone, 7 days post lesion (dpl). Treatments were repeated once a week at 14, 21, 28, and 35 dpl.

Behavioral impairment was evaluated by two separate observers blind to the treatment analyzing the hind limb posture and gait capability, and assigning a clinical score in accordance with the following criteria described by Albano et al. [47, 48]. Animals were sacrificed at 42 dpl by intracardial

perfusion and organs, i.e. spinal cords and GMs were dissected out, post-fixed, embedded in OCT or paraffin, respectively, and sectioned using a cryostat or a microtome.

**Open field grid walk test**

Open field grid walk test for motor coordination impairment was performed at 7, 21, and 42 dpl using a “tracking camera” placed above the open field, to record and quantify the distance covered by every animal and a “counting camera”, placed in line with the grid, to quantify the number of footfalls within 2 min. For each performance, each animal was placed in a  $40 \times 40 \text{ cm}$  grid (each mesh  $1 \text{ cm}^2$ ) and was free to move and explore during the behavioral test. The tracking and the counting videos were analyzed offline using Ctrax tracker software version 0.5.18 for Mac.

**Electromyography**

EMG analysis was performed at 42 dpl using a portable two-channel EMG device (Myoquick, Micromed S.p.A., Mogliano Veneto, Treviso, Italy) with one bipolar concentric needle electrode inserted in the left GM and one ground electrode. Animals were anesthetized with isoflurane before the electromyographic recording. The spontaneous electrical activity of the muscle was recorded and then analyzed using System PLUS Evolution software by Micromed S.p.A. (Mogliano Veneto, Treviso, Italy).

**mRNA analysis**

For quantification of mRNA levels of Dnm1l and actb in muscle, we used the QuantiGene Plex Magnetic Separation Assay kit (Affymetrix, Santa Clara, CA, USA) following the manufacturer’s instructions and as previously described [32]. The signal was detected with a Luminex instrument (Bio-Rad, Milan, Italy). For each sample, the average signal (MFI) for Dnm1l and actb were determined and, after average background signal subtraction, Dnm1l signal was normalized to the housekeeping gene signal.

### Immunohistochemistry

Rehydrated sections were subjected to a standard protocol of immunohistochemistry. Both muscle and spinal cord sections were subjected to a protocol of antigen retrieval (for AChE, Gfap and F4/80 staining) using an antigen retrieval buffer (0.1% Tween 20 in citrate buffer solution) and heating in microwave (5 min per 3 cycles). After samples were blocked with 3% H<sub>2</sub>O<sub>2</sub> in PBS for 15 min at room temperature in a humidity chamber, they were washed in PBS and incubated for 40 min at room temperature in a humidity chamber with the following primary antibodies diluted in 0.3% Triton X100 in PBS: rat monoclonal anti-F4/80 (Bio-Rad, Cat#MCA497R, RRID: 323279, 1:100), rabbit monoclonal anti-AChE (Abcam, Cat#ab240274, RRID: AB\_2857345, 1:50), mouse monoclonal anti-GFAP (BD Biosciences, Cat#610566, RRID: AB\_397916, 1:100). Then, samples were washed in 0.3% Triton in PBS three times for 5 min and incubated with pre-diluted biotinylated secondary antibody (Vector Laboratories, Burlingame, CA) and with R.T.U. VECTASTAIN Elite ABC Reagent (Vector Laboratories) for 30 min at room temperature in a humidity chamber, respectively. Samples were then washed in 0.3% Triton X100 in PBS for 5 min and exposed to a solution of 1% DAB, 0.3% H<sub>2</sub>O<sub>2</sub> in PBS. Nuclei were counterstained with Mayer's hematoxylin (Bio-Optica), dehydrated with increasing concentration of ethanol (70%, 95%, 100%) and xylene, and coverslipped with Entellan (Merck, Cat# 1.079.600.500).

For the analysis of GFAP by immunohistochemistry on the spinal cord, sections were counterstained with cresyl violet staining, dehydrated with the same procedure above and coverslipped with BrightMount (Aqueous Mounting Medium for Fluorescent Staining, Abcam, Cat#ab103746).

For neuronal or muscle fiber staining, spinal cord and muscle sections were stained with cresyl violet or hematoxylin/eosin, respectively.

For quantification of the number of GFAP positive cells, muscle fibers diameter distribution, CNL and F4/80 positive cells,  $n \geq 3$  equally spaced sections of the spinal cord or GM were analyzed and quantified by operators blind to the treatment using an Olympus BH2 microscope and Olympus CAST GRID software.

### Immunofluorescence

After antigen retrieval procedure as described above, sections were incubated with 10% NGS in PBS–0.3% Triton for 1 h at room temperature and then overnight at 4 °C with an appropriate combination of one of the following antibodies diluted in 1% NGS in PBS and 0.3% Triton. For spinal cord staining: rabbit polyclonal anti-Gli1 (Abcam, Cat#ab49314, RRID: AB\_880198, 1:100); mouse monoclonal anti-NeuN (Millipore, Cat#MAB377, RRID: AB\_2298772, 1:100); mouse monoclonal anti-GFAP (BD Biosciences, Cat# 610566, RRID: AB\_397916, 1:500); goat polyclonal anti-ALF1/IBA1 (Novus, Cat# NB100-1028, RRID: AB\_521594, 1:100); rabbit polyclonal anti-SYP (Santa Cruz Biotechnology, Cat#sc-9116, RRID: AB\_2199007, 1:50); rabbit monoclonal anti-P-Stat3 (Cell signaling Technology, Cat# 9145, RRID: AB\_2491009, 1:200). For muscle staining: mouse monoclonal anti-PAX7 (Abcam, Cat# ab199010, RRID: N.A., 1:250); rat monoclonal anti-F4/80 (Bio-Rad, Cat# MCA497R, RRID: AB\_323279, 1:50); mouse monoclonal anti-iNOS (Santa Cruz Biotechnology, Cat# sc-7271, RRID: AB\_627810, 1:50); rabbit polyclonal anti-ARG1 (Santa Cruz Biotechnology, Cat# sc-20150, RRID: AB\_2958955, 1:50); mouse monoclonal anti-DRP1 (BD Biosciences, Cat# 611112, RRID: AB\_398423, 1:100). Samples were then washed and incubated for 1 h at room temperature with appropriate secondary antibodies diluted 1:1000 in 1% NGS in PBS and 0.3% Triton: donkey anti-goat (Alexa Fluor 488, ThermoFisher Scientific, Cat#A-11055, RRID: AB\_2534102 or Alexa Fluor 546, ThermoFisher Scientific, Cat#A-11056, RRID: AB\_142628); goat polyclonal anti-rabbit (Alexa Fluor 488, Molecular Probes, Cat#A-11008, RRID: AB\_143165; Alexa Fluor 546, Molecular Probes, Cat# A-11010, RRID: AB\_2534077; Alexa Fluor 647, ThermoFisher Scientific, Cat#A-21244, RRID: AB\_2535812); goat polyclonal anti-mouse (Alexa Fluor 488, ThermoFisher Scientific, Cat# A-11001, RRID: AB\_2534069; Alexa Fluor 546, Molecular Probes, Cat#A-11003, RRID: AB\_141370; Alexa Fluor 647, ThermoFisher Scientific, Cat# A-21235, RRID: AB\_2535804); goat anti-rat (Alexa Fluor 488, Molecular Probes, Cat# A-11006, RRID: AB\_141373). Nuclei were counterstained with DAPI 1:1000 in PBS. Slides were coverslipped with BrightMount (Abcam, Cat#ab103746).

For quantification of Gli1 fluorescence intensity (FI), Gli1 nuclear FI, iNOS FI, Arg1 FI, and mitochondrial length  $n \geq 5$  regions of interest per  $n \geq 3$  sections per animal were analyzed and quantified by operators blinded to the treatment using ImageJ v. 2.1.0/1.53c (Fiji) software.

### Flow cytometry

Flow cytometry analysis was performed on fresh tissues. Isolated spinal cords were kept in a cold IMDM medium supplemented with 5% FBS, 1%

GlutaMAX, and 1% pen/strep and mechanically minced. Samples were then enzymatically digested at 37 °C for 30 min with a cocktail of 2 mg/ml collagenase IV, 0.2 mg/ml dispase, and 0.1 mg/ml DNase I in supplemented IMDM. Then, the cell suspension was homogenized by passing through 40  $\mu$ m cell strainers using 10 ml of supplemented IMDM for sample. For myelin removal, the suspension was mixed with 90% isotonic Percoll diluted in PBS 10x and then centrifuged for 20 min at 800xg. Cell pellet was resuspended in cold buffer (MACS BSA diluted in autoMACS rinsing solution) and centrifuged twice at 4 °C for 5 min at 300g, resuspending pellet with cold buffer and flow cytometry staining buffer respectively, obtaining 1,000,000 cells/100  $\mu$ l/sample. Samples were finally incubated for 15 min at 4 °C with the following monoclonal antibodies: anti-mouse CD45 (Miltenyi Biotech, Cat#130-110-802, RRID: AB\_2658222), CD11b (Miltenyi Biotech, Cat#130-113-803, RRID: AB\_2819369), F4/80 (Biolegend, Cat#123118, RRID: AB\_893477), Ly-6G (Miltenyi Biotech, Cat#130-117-500, RRID: AB\_2727967), CCR2 (Miltenyi Biotech, Cat#130-117-548, RRID: AB\_2727981), CX3CR1 (Biolegend, Cat#149006, RRID: AB\_2564315), CD206 (Biolegend, Cat#141717, RRID: AB\_2562232), and CD80 (Miltenyi Biotech, Cat#130-116-462, RRID: AB\_2727559) antibodies.

In all experiments, viability fixable dye (Miltenyi Biotech, Cat#130-109-816) was used to label dead cells. Data were collected on a MACSQuant Analyzer (Miltenyi Biotech) and analyzed using Flowlogic software (Miltenyi Biotech).

Data analysis was performed as described elsewhere [49, 50]. Briefly, it was based on a multi-step bioinformatics approach: (1) reading FCS data; (2) building a self-organizing map (SOM) for clustering; (3) performing a dimensionality reduction through principal component analysis (PCA) and uniform manifold approximation and projection (UMAP); (4) perform a supervised identification of each cluster; (5) performing a statistical analysis on the abundance of each population according to their origin (ANOVA). Besides the characterization of the myeloid compartment, the unsupervised clustering algorithm identified two different lymphocytes clusters: one with strong positivity for HLA-DR, that we identified as B cells and a second one that includes residual T and NK cells (T/NK) which cannot be separated with the current markers panel.

### Tissue preparation and HPLC analysis of metabolites

All animals of the three groups (controls, CTB-Sap vehicle, and CTB-Sap colobatosol) underwent the same surgical procedure to remove spinal cord and GMs. Once removed, tissues were immediately immersed in liquid nitrogen, weighed and deproteinized by homogenization in ice-cold HPLC-grade CH<sub>3</sub>CN + 10 mM KH<sub>2</sub>PO<sub>4</sub> pH 7.40 (3:1; v-v), using an Ultra-Turrax (Janke and Kunkel, Staufen, Germany) at 24,000 rpm/min for 90 s [51–55]. Following centrifugation at 20,690xg for 10 min at 4 °C, clear supernatants were supplemented with HPLC-grade chloroform, vigorously agitated and centrifuged for 5 min in a top-bench centrifuge at the maximal speed. The upper aqueous phase was used for the HPLC analyses of metabolites. The simultaneous separation and quantification of high-energy phosphates, oxidized and reduced nicotinic coenzymes, purines, pyrimidines, antioxidants, oxidative/nitrosative stress biomarkers and N-acetylaspartate (NAA) was performed as described in detail elsewhere. Amino acids (AA) and amino group-containing compounds (AGCC) were separated and quantified according to chromatographic conditions previously set up in our laboratory. In both cases, the HPLC apparatus consisted of a Spectra System P4000 pump, connected to a Hypersil C-18 250  $\times$  4.6 mm, 5  $\mu$ m particle size column (provided with its own guard column) and to a highly sensitive UV6000 LP diode array detector equipped with a 5 cm light path flow cell (ThermoFisher Scientific, Rodano, Milano, Italy). Overall, the two analyses allowed measuring the concentrations of 61 water-soluble low molecular weight compounds in tissue extracts, thanks to the comparisons with appropriate ultrapure standard mixtures with known concentrations.

### Principal components analysis

Principal components analysis (PCA) was performed on spinal cord and GMs metabolites data. Explained variances and the quality of representation of the variables on the factor map expressed as square cosine (Cos<sup>2</sup>) are shown. PCA is expressed as a biplot of variables and key-colored arrows representing each variable are also shown. Analyses were carried out using the RStudio software (Version 1.0.153, for Mac), fitted with corr plot, FactoMineR, and Factoextra packages for computing and visualizing PCA diagrams.

### Human gene expression

For human ALS data, we used the NCBI Gene Expression Omnibus (GEO) database (<http://www.ncbi.nlm.nih.gov/geo/>) to select  $n = 10$  healthy and



$n = 10$  ALS patients cervical spinal cord transcriptome dataset (GSE26927) analyzing the expression levels of  $n = 6$  selected genes (i.e. PTCH1, SMO, SHH, GLI2, GLI1, and GLI3). Mesh terms "Spinal Cord", "ALS" and "Human" were used to identify potential datasets of interest. The dataset selected was downloaded and analyzed using MultiExperiment Viewer (MeV) software. Statistical analysis was performed using GraphPad Prism software version 5.00 for Mac and MeV software. Interaction network of SHH signaling pathway was obtained using String (<https://string-db.org/>) online tool for gene ontology and KEGG enrichment analysis.

#### Quantification and statistical analysis

The sample size for each experiment is reported in figure legends. No statistical methods were used to predetermine sample sizes, but our sample sizes were similar to those reported in previous publications [15, 18, 48, 56]. Mice were randomly assigned to experimental groups. No data points or animals were excluded from the analysis. For statistical analyses, a two-tailed unpaired Student's *t*-test was used for comparison of  $n = 2$  groups. For comparison of  $n \geq 3$  groups, one-way or two-way analysis of variance (ANOVA), or repeated-measures ANOVA with Holm–Sidak post-hoc test for multiple comparisons were used where appropriate. Data are presented as the mean  $\pm$  standard error of the mean (SEM) unless otherwise stated. Data analysis was performed using GraphPad Prism software version 5.00 or RStudio software version 1.0.153. A value of  $p < 0.05$  was considered statistically significant and symbols used to indicate statistical differences are described in figure legends.

#### DATA AVAILABILITY

The datasets used and/or analyzed during the current study are available from the corresponding author on reasonable request.

#### REFERENCES

- Glass CK, Saijo K, Winner B, Marchetto MC, Gage FH. Mechanisms underlying inflammation in neurodegeneration. *Cell* 2010;140:918–34.
- Chio A, Logroscino G, Hardiman O, Swinger R, Mitchell D, Beghi E, et al. Prognostic factors in ALS: a critical review. *Amyotroph Lateral Scler*. 2009;10:310–23.
- Liscic RM, Alberici A, Cairns NJ, Romano M, Buratti E. From basic research to the clinic: innovative therapies for ALS and FTD in the pipeline. *Mol Neurodegener*. 2020;15:31.
- Buratti E. Targeting TDP-43 proteinopathy with drugs and drug-like small molecules. *Br J Pharmacol*. 2020;178:1298–1315.
- McGoldrick P, Joyce PI, Fisher EM, Greensmith L. Rodent models of amyotrophic lateral sclerosis. *Biochim Biophys Acta*. 2013;1832:1421–36.
- Hardiman O, Al-Chalabi A, Chio A, Corr EM, Logroscino G, Robberecht W, et al. Amyotrophic lateral sclerosis. *Nat Rev Dis Prim*. 2017;3:17071.
- Korner S, Kollwe K, Fahlbusch M, Zapf A, Dengler R, Krampfl K, et al. Onset and spreading patterns of upper and lower motor neuron symptoms in amyotrophic lateral sclerosis. *Muscle Nerve*. 2011;43:636–42.
- Fischer LR, Culver DG, Tennant P, Davis AA, Wang M, Castellano-Sanchez A, et al. Amyotrophic lateral sclerosis is a distal axonopathy: evidence in mice and man. *Exp Neurol*. 2004;185:232–40.
- Moloney EB, de Winter F, Verhaagen J. ALS as a distal axonopathy: molecular mechanisms affecting neuromuscular junction stability in the presymptomatic stages of the disease. *Front Neurosci*. 2014;8:252.
- Frey D, Schneider C, Xu L, Borg J, Spooren W, Caroni P. Early and selective loss of neuromuscular synapse subtypes with low sprouting competence in motoneuron diseases. *J Neurosci*. 2000;20:2534–42.
- Troger M, Dengler R. The role of electromyography (EMG) in the diagnosis of ALS. *Amyotroph Lateral Scler Other Mot Neuron Disord*. 2000;1(Suppl. 2):S33–40.
- Nichols NL, Vinit S, Bauernschmidt L, Mitchell GS. Respiratory function after selective respiratory motor neuron death from intrapleural CTB-saporin injections. *Exp Neurol*. 2015;267:18–29.
- Lind LA, Murphy ER, Lever TE, Nichols NL. Hypoglossal motor neuron death via intralingual CTB-saporin (CTB-SAP) injections mimic aspects of amyotrophic lateral sclerosis (ALS) related to dysphagia. *Neuroscience* 2018;390:303–16.
- Gulino R, Perciavalle V, Gulisano M. Expression of cell fate determinants and plastic changes after neurotoxic lesion of adult mice spinal cord by cholera toxin-B saporin. *Eur J Neurosci*. 2010;31:1423–34.
- Gulino R, Vicario N, Giunta MAS, Spoto G, Calabrese G, Vecchio M, et al. Neuromuscular plasticity in a mouse neurotoxic model of spinal motoneuronal loss. *Int J Mol Sci*. 2019;20:1500.
- McGeer PL, McGeer EG. Inflammatory processes in amyotrophic lateral sclerosis. *Muscle Nerve*. 2002;26:459–70.
- Van Dyke JM, Smit-Ostad IM, Macrander C, Krakora D, Meyer MG, Suzuki M. Macrophage-mediated inflammation and glial response in the skeletal muscle of a rat model of familial amyotrophic lateral sclerosis (ALS). *Exp Neurol*. 2016;277:275–82.
- Giusto E, Codrich M, de Leo G, Francardo V, Coradazzi M, Parenti R, et al. Compensatory changes in degenerating spinal motoneurons sustain functional sparing in the SOD1-G93A mouse model of amyotrophic lateral sclerosis. *J Comp Neurol*. 2020;528:231–43.
- Bambakidis NC, Petrullis M, Kui X, Rothstein B, Karampelas I, Kuang Y, et al. Improvement of neurological recovery and stimulation of neural progenitor cell proliferation by intrathecal administration of Sonic hedgehog. *J Neurosurg*. 2012;116:1114–20.
- Ma X, Turnbull P, Peterson R, Turnbull J. Trophic and proliferative effects of Shh on motor neurons in embryonic spinal cord culture from wildtype and G93A SOD1 mice. *BMC Neurosci*. 2013;14:119.
- Pitter KL, Tamagno I, Feng X, Ghosal K, Amankulor N, Holland EC, et al. The SHH/Gli pathway is reactivated in reactive glia and drives proliferation in response to neurodegeneration-induced lesions. *Glia* 2014;62:1595–607.
- Loulier K, Ruat M, Traiffort E. Increase of proliferating oligodendroglial progenitors in the adult mouse brain upon Sonic hedgehog delivery in the lateral ventricle. *J Neurochem*. 2006;98:530–42.
- Fuccillo M, Joyner AL, Fishell G. Morphogen to mitogen: the multiple roles of hedgehog signalling in vertebrate neural development. *Nat Rev Neurosci*. 2006;7:772–83.
- Lai K, Kaspar BK, Gage FH, Schaffer DV. Sonic hedgehog regulates adult neural progenitor proliferation in vitro and in vivo. *Nat Neurosci*. 2003;6:21–7.
- Belgacem YH, Hamilton AM, Shim S, Spencer KA, Borodinsky LN. The many hats of sonic hedgehog signaling in nervous system development and disease. *J Dev Biol*. 2016;4:35.
- Drannik A, Martin J, Peterson R, Ma X, Jiang F, Turnbull J. Cerebrospinal fluid from patients with amyotrophic lateral sclerosis inhibits sonic hedgehog function. *PLoS ONE*. 2017;12:e0171668.
- Stanton BZ, Peng LF. Small-molecule modulators of the Sonic Hedgehog signaling pathway. *Mol Biosyst*. 2010;6:44–54.
- Chechneva OV, Mayrhofer F, Daugherty DJ, Krishnamurthy RG, Bannerman P, Pleasure DE, et al. A smoothened receptor agonist is neuroprotective and promotes regeneration after ischemic brain injury. *Cell Death Dis*. 2014;5:e1481.
- Ruat M, Hoch L, Faure H, Rognan D. Targeting of smoothened for therapeutic gain. *Trends Pharm Sci*. 2014;35:237–46.
- Najm FJ, Madhavan M, Zaremba A, Shick E, Karl RT, Factor DC, et al. Drug-based modulation of endogenous stem cells promotes functional remyelination in vivo. *Nature* 2015;522:216–20.
- Wang J, Lu J, Bond MC, Chen M, Ren XR, Lyerly HK, et al. Identification of select glucocorticoids as smoothened agonists: potential utility for regenerative medicine. *Proc Natl Acad Sci USA*. 2010;107:9323–8.
- Vicario N, Bernstock JD, Spitalo FM, Giallongo C, Giunta MAS, Li Volti G, et al. Clobetasol modulates adult neural stem cell growth via canonical hedgehog pathway activation. *Int J Mol Sci*. 2019;20:1991.
- Bories C, Amendola J, Lamotte d'Incamps B, Durand J. Early electrophysiological abnormalities in lumbar motoneurons in a transgenic mouse model of amyotrophic lateral sclerosis. *Eur J Neurosci*. 2007;25:451–9.
- Durand J, Amendola J, Bories C, Lamotte d'Incamps B. Early abnormalities in transgenic mouse models of amyotrophic lateral sclerosis. *J Physiol Paris*. 2006;99:211–20.
- Gulino R, Dimartino M, Casabona A, Lombardo SA, Perciavalle V. Synaptic plasticity modulates the spontaneous recovery of locomotion after spinal cord hemisection. *Neurosci Res*. 2007;57:148–56.
- Gulino R, Gulisano M. Noggin and Sonic hedgehog are involved in compensatory changes within the motoneuron-depleted mouse spinal cord. *J Neurol Sci*. 2013;332:102–9.
- Blasco H, Lanzaster D, Veyrat-Durebex C, Hergesheimer R, Vourch P, Maillot F, et al. Understanding and managing metabolic dysfunction in amyotrophic lateral sclerosis. *Expert Rev Neurother*. 2020;20:907–19.
- Valbuena GN, Cantoni L, Tortorolo M, Bendotti C, Keun HC. Spinal cord metabolic signatures in models of fast- and slow-progressing SOD1(G93A) amyotrophic lateral sclerosis. *Front Neurosci*. 2019;13:1276.
- Yoshino H, Edaravone for the treatment of amyotrophic lateral sclerosis. *Expert Rev Neurother*. 2019;19:185–93.
- Folker ES, Baylies MK. Nuclear positioning in muscle development and disease. *Front Physiol*. 2013;4:363.
- Lunetta C, Lizio A, Tremolizzo L, Ruscica M, Macchi C, Riva N, et al. Serum irisin is upregulated in patients affected by amyotrophic lateral sclerosis and correlates with functional and metabolic status. *J Neurol*. 2018;265:3001–8.
- Gonzalez D, Contreras O, Rebolledo DL, Espinoza JP, van Zundert B, Brandan E. ALS skeletal muscle shows enhanced TGF- $\beta$  signaling, fibrosis and induction of fibro/adipogenic progenitor markers. *PLoS ONE*. 2017;12:e0177649.

43. Dupuis L, Corcia P, Fergani A, Gonzalez De Aguilar JL, Bonnefont-Rousselot D, Bittar R, et al. Dyslipidemia is a protective factor in amyotrophic lateral sclerosis. *Neurology* 2008;70:1004–9.
44. Hollinger SK, Okosun IS, Mitchell CS. Antecedent disease and amyotrophic lateral sclerosis: what is protecting whom? *Front Neurol*. 2016;7:47.
45. Gulino R, Parenti R, Gulisano M. Novel mechanisms of spinal cord plasticity in a mouse model of motoneuron disease. *Biomed Res Int*. 2015;2015:654637.
46. Gulino R, Forte S, Parenti R, Gulisano M. TDP-43 as a modulator of synaptic plasticity in a mouse model of spinal motoneuron degeneration. *CNS Neurol Disord Drug Targets*. 2015;14:55–60.
47. Albano R, Liu X, Lobner D. Regulation of system x(c)- in the SOD1-G93A mouse model of ALS. *Exp Neurol*. 2013;250:69–73.
48. Spitale FM, Vicario N, Rosa MD, Tibullo D, Vecchio M, Gulino R, et al. Increased expression of connexin 43 in a mouse model of spinal motoneuronal loss. *Aging*. 2020;12:12598–608.
49. Perez C, Botta C, Zabaleta A, Puig N, Cedena MT, Goicoechea I, et al. Immunogenomic identification and characterization of granulocytic myeloid-derived suppressor cells in multiple myeloma. *Blood* 2020;136:199–209.
50. Maia C, Martin-Sanchez E, Garces JJ, De Cerio AL, Inoges S, Landecho MF, et al. Immunologic characterization of COVID-19 patients with hematological cancer. *Haematologica*. 2020;106:1457–60.
51. Lazzarino G, Amorini AM, Fazzina G, Vagnozzi R, Signoretti S, Donzelli S, et al. Single-sample preparation for simultaneous cellular redox and energy state determination. *Anal Biochem*. 2003;322:51–9.
52. Belli A, Sen J, Petzold A, Russo S, Kitchen N, Smith M, et al. Extracellular N-acetylaspartate depletion in traumatic brain injury. *J Neurochem*. 2006;96:861–9.
53. Bracko O, Di Pietro V, Lazzarino G, Amorini AM, Tavazzi B, Artmann J, et al. 3-Nitropropionic acid-induced ischemia tolerance in the rat brain is mediated by reduced metabolic activity and cerebral blood flow. *J Cereb Blood Flow Metab*. 2014;34:1522–30.
54. Amorini AM, Giorlandino C, Longo S, D'Urso S, Mesoraca A, Santoro ML, et al. Metabolic profile of amniotic fluid as a biochemical tool to screen for inborn errors of metabolism and fetal anomalies. *Mol Cell Biochem*. 2012;359:205–16.
55. Lazzarino G, Amorini AM, Barnes NM, Bruce L, Mordente A, Lazzarino G, et al. Low molecular weight dextran sulfate (ILB(R)) administration restores brain energy metabolism following severe traumatic brain injury in the rat. *Antioxidants*. 2020;9:850.
56. Vicario N, Pasquincucci L, Spitale FM, Chiechio S, Turnaturi R, Caraci F, et al. Simultaneous activation of Mu and Delta opioid receptors reduces allodynia and astrocytic Connexin 43 in an animal model of neuropathic pain. *Mol Neurobiol*. 2019;56:7338–54.

#### ACKNOWLEDGEMENTS

The authors acknowledge the Center for Advanced Preclinical in vivo Research (CAPIR) and the confocal microscopy facility at the Bio-Nanotech Research and Innovation Tower (BRIT) of the University of Catania, for the technical contribution of the staff.

#### AUTHOR CONTRIBUTIONS

Conceptualization: NV, RP, RG; Project administration: NV, FMS, DT, RP, RG; Methodology: NV, FMS, DT, CG, AMA, RM, CB, MV, MDR, GLV, GLa, RP, RG; Investigation: NV, FMS, DT, CG, AMA, GSc, GSp, MWS, SDA, CA, MV, MDR, RG; Formal analysis: NV, FMS, DT, CG, AMA, JDB, CB, MG, GLe, RZ, MV, MDR, GLV, GLa, RP, RG; Resources: DT, AMA, MG, MV, MDR, GLV, GLa, RP, RG; Supervision: NV, GLV, GLa, RP,

RG; Writing—Original Draft: NV, FMS, RP, RG; Writing—Reviewing and Editing: NV, FMS, DT, CG, JDB, CB, MG, EB, GLe, RZ, GLV, GLa, RP, RG.

#### FUNDING

NV was supported by the PON AIM R&I 2014-2020-E66C18001240007. FMS was supported by the International Ph.D. program in Neuroscience and PO FSE 2014–2020 Fellowship (Department of Biomedical and Biotechnological Sciences, University of Catania, Italy). RZ is supported by the Slovenian Research Agency grant #P3-310. This study was partially funded by grants from the Italian Ministero dell'Istruzione, dell'Università e della Ricerca, PRIN 2017, Grant no. 2017XKWWK9\_004 and PRIN 2015, Grant. no. 2015MJBEM2\_006 to RP and RG.

#### ETHICS STATEMENT

The study was conducted in accordance with the recommendations of the local committee for animal welfare (OPBA, University of Catania, Via Santa Sofia 97, Catania, Italy); the protocol was approved by OPBA and by the Italian Ministry of Health.

#### COMPETING INTERESTS

JDB has positions/equity in POKKIT Diagnostics, Trevivir LLC, and Avidea Technologies.

#### ADDITIONAL INFORMATION

**Supplementary information** The online version contains supplementary material available at <https://doi.org/10.1038/s41419-021-03907-1>.

**Correspondence** and requests for materials should be addressed to N.V., R.P. or R.G.

**Reprints and permission information** is available at <http://www.nature.com/reprints>

**Publisher's note** Springer Nature remains neutral with regard to jurisdictional claims in published maps and institutional affiliations.



**Open Access** This article is licensed under a Creative Commons Attribution 4.0 International License, which permits use, sharing, adaptation, distribution and reproduction in any medium or format, as long as you give appropriate credit to the original author(s) and the source, provide a link to the Creative Commons license, and indicate if changes were made. The images or other third party material in this article are included in the article's Creative Commons license, unless indicated otherwise in a credit line to the material. If material is not included in the article's Creative Commons license and your intended use is not permitted by statutory regulation or exceeds the permitted use, you will need to obtain permission directly from the copyright holder. To view a copy of this license, visit <http://creativecommons.org/licenses/by/4.0/>.

© The Author(s) 2021

Supplementary figures and figure legends for:

**Clobetasol promotes neuromuscular plasticity in mice after motoneuronal loss via sonic hedgehog signaling, immunomodulation and metabolic rebalancing**

Nunzio Vicario, Federica M. Spitale, Daniele Tibullo, Cesarina Giallongo, Angela M. Amorini, Grazia Scandura, Graziana Spoto, Miriam W. Saab, Simona D'Aprile, Cristiana Alberghina, Renata Mangione, Joshua D. Bernstock, Cirino Botta, Massimo Gulisano, Emanuele Buratti, Giampiero Leanza, Robert Zorec, Michele Vecchio, Michelino Di Rosa, Giovanni Li Volti, Giuseppe Lazzarino, Rosalba Parenti, Rosario Gulino.

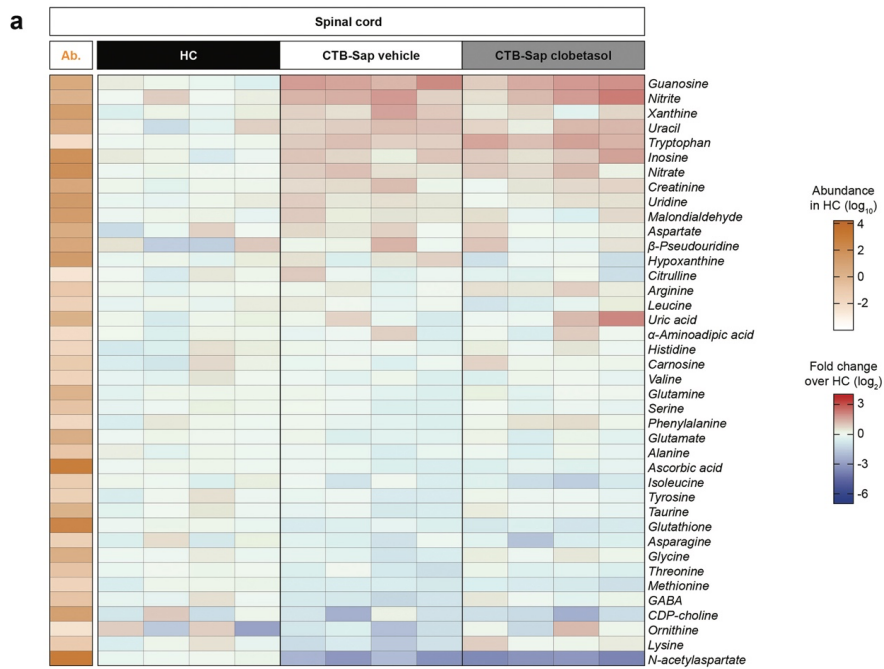


**Fig. S1 | Clobetasol modifies metabolism of MN-depleted spinal cord.** a, Heat maps of 40 metabolites in HC, CTB-Sap vehicle and CTB-Sap clobetasol spinal cord at 42 dpl showing the abundance (Ab.) in HC and the relative

changes in CTB-Sap vehicle and CTB-Sap clobetasol as compared to HC; data are shown  $\log_{10}$  abundance and  $\log_2$  FC over HC of n = 4 mice per group.

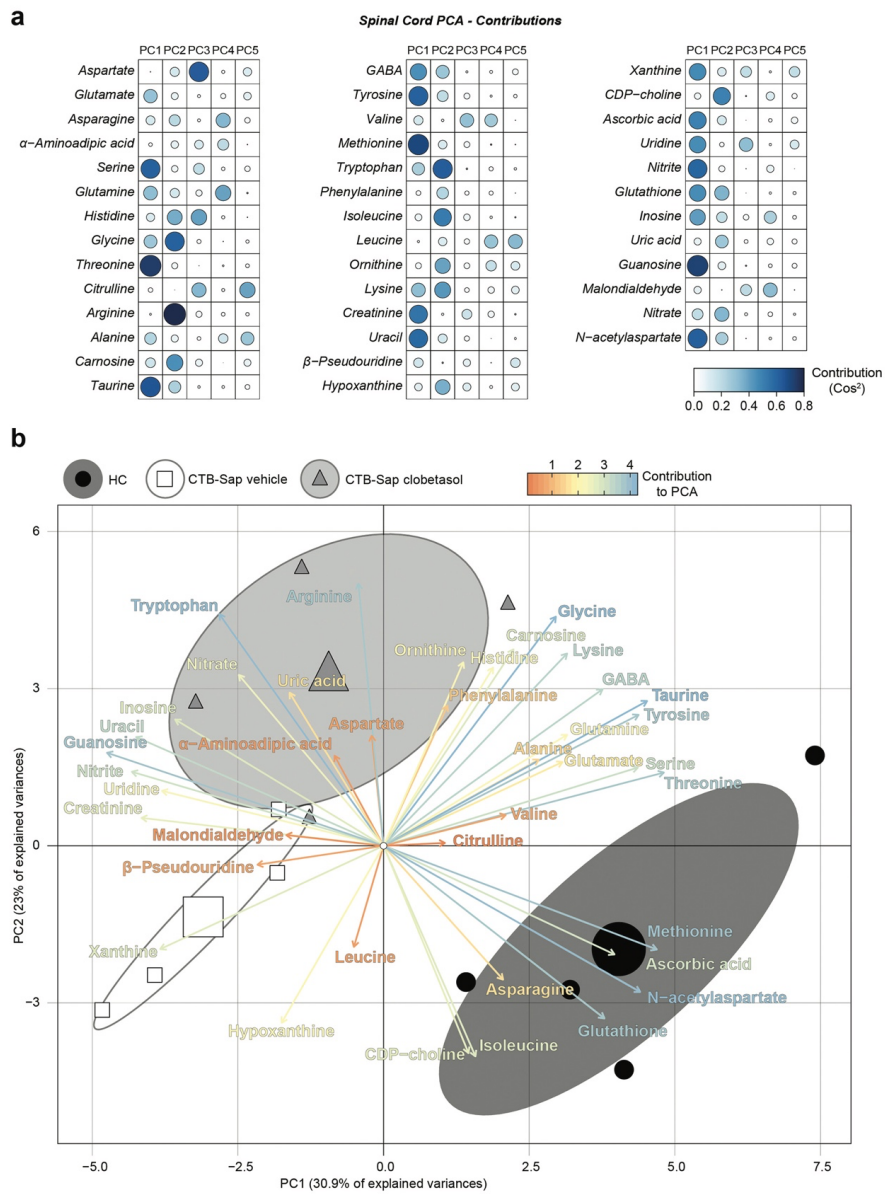


**Fig. S2 | Principal components analysis (PCA) of spinal cord metabolites in HC, CTB-Sap vehicle and CTB-Sap clobetasol mice. a.** Factor map of quality plot representation of the variables on PC1-PC5 expressed as square cosine (Cos<sup>2</sup>). **b.** PCA biplot of 40 metabolites for HC,

CTB-Sap vehicle and CTB-Sap clobetasol; key-colored arrows represent the contribution of each variable to the PCA; small circles/squares/triangles represent single subjects and large circles/squares/triangles represents the mean point of the confidence ellipses.

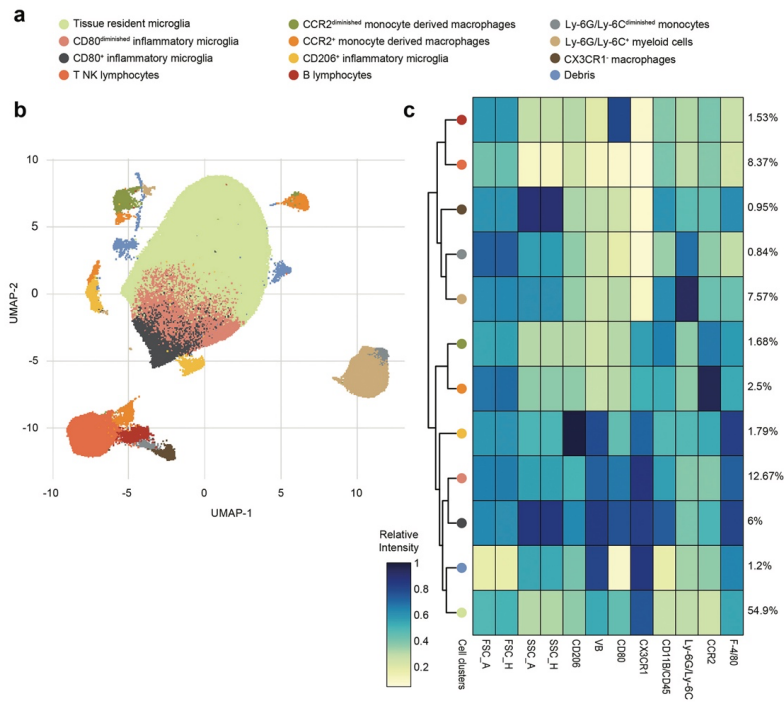


**Fig. S3 | Cell populations identified by multi-step bioinformatics analysis of flow cytometry panel. a, b.** Uniform Manifold Approximation and Projection (UMAP) representation of the populations identified through flow-cytometry by “fusing” all the events from the 12 samples (4 mice for 3 conditions).

**c.** Heatmap showing the expression of each marker in each population. The differential expression was used to assign, in a supervised manner, each cluster to each immune population. The overall abundance of each subpopulation is reported within the heatmap.

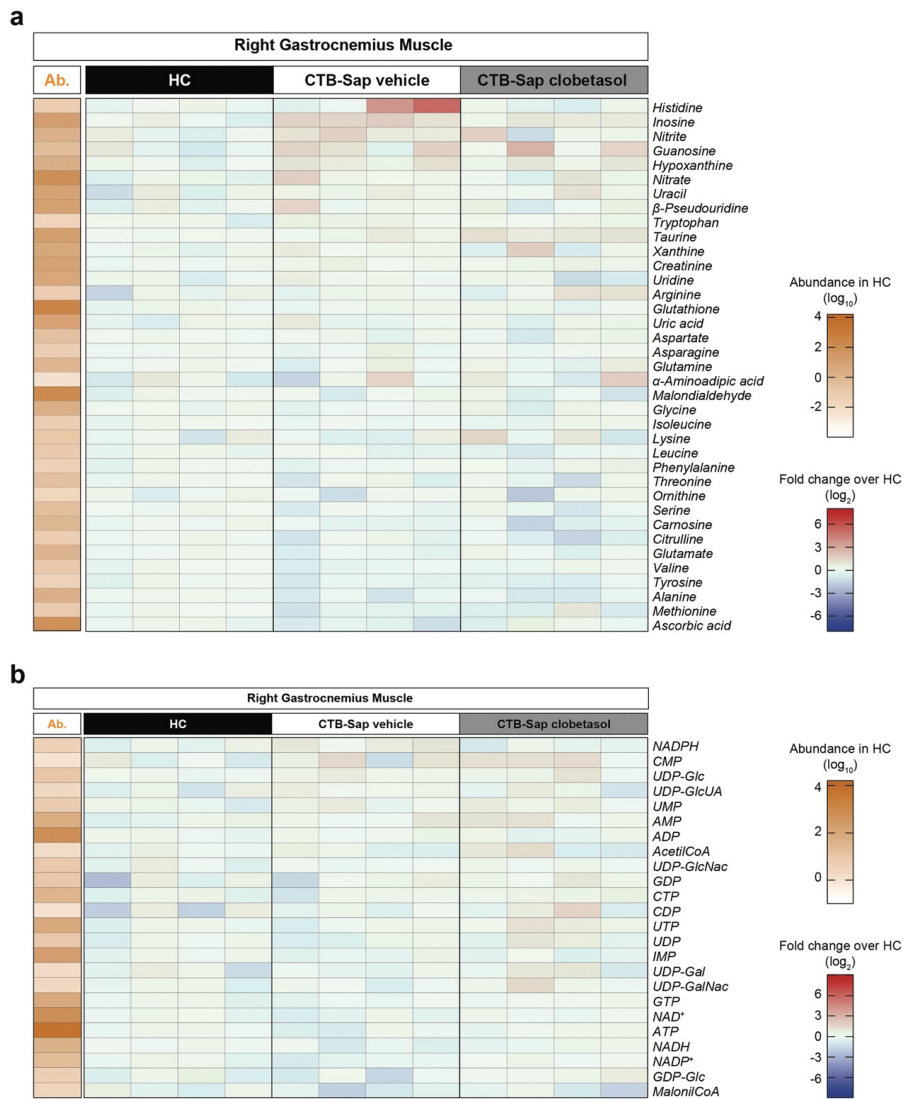


**Fig. S4 | Effects of clobetasol onto contralateral, unaffected muscle. a,** Heat maps of 37 metabolites in the right GM HC, CTB-Sap vehicle and CTB-Sap clobetasol at 42 dpl showing the abundance (Ab.) in HC and the relative changes in CTB-Sap vehicle and CTB-Sap clobetasol as compared to HC; data are shown as  $\log_{10}$  abundance and  $\log_2$  FC over HC of  $n = 4$  mice per group.

**b,** Heat maps of 24 metabolites in the right GM HC, CTB-Sap vehicle and CTB-Sap clobetasol at 42 dpl showing the abundance (Ab.) in HC and the relative changes in CTB-Sap vehicle and CTB-Sap clobetasol as compared to HC; data are shown as  $\log_{10}$  abundance and  $\log_2$  FC over HC of  $n = 4$  mice per group.

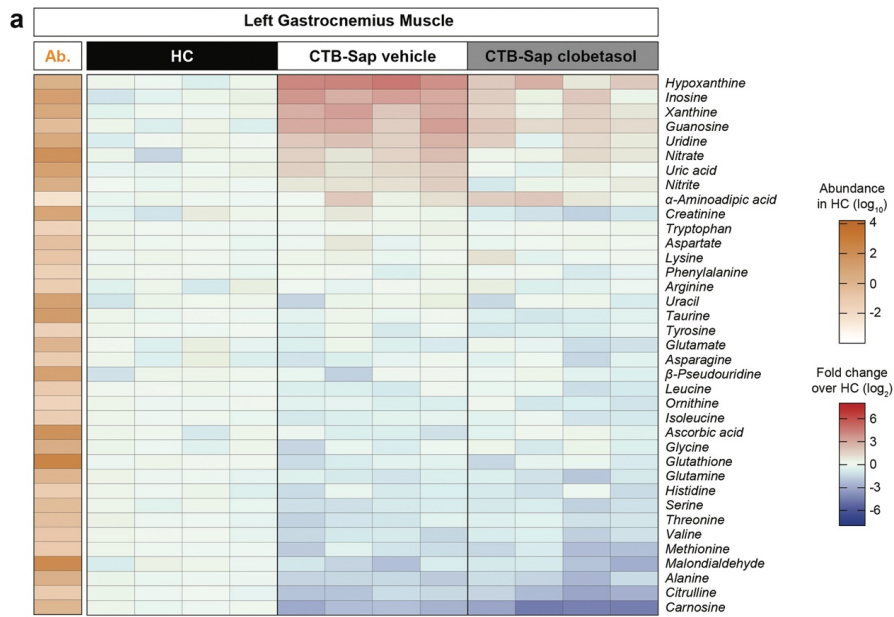


**Fig. S5. Clobetasol modifies metabolism of denervated muscle.** a, Heat maps of 37 metabolites in the left GM HC, CTB-Sap vehicle and CTB-Sap clobetasol at 42 dpi showing the abundance (Ab.) in HC and the relative

changes in CTB-Sap vehicle and CTB-Sap clobetasol as compared to HC; data are shown as  $\log_{10}$  abundance and  $\log_2$  FC over HC of  $n = 4$  mice per group.

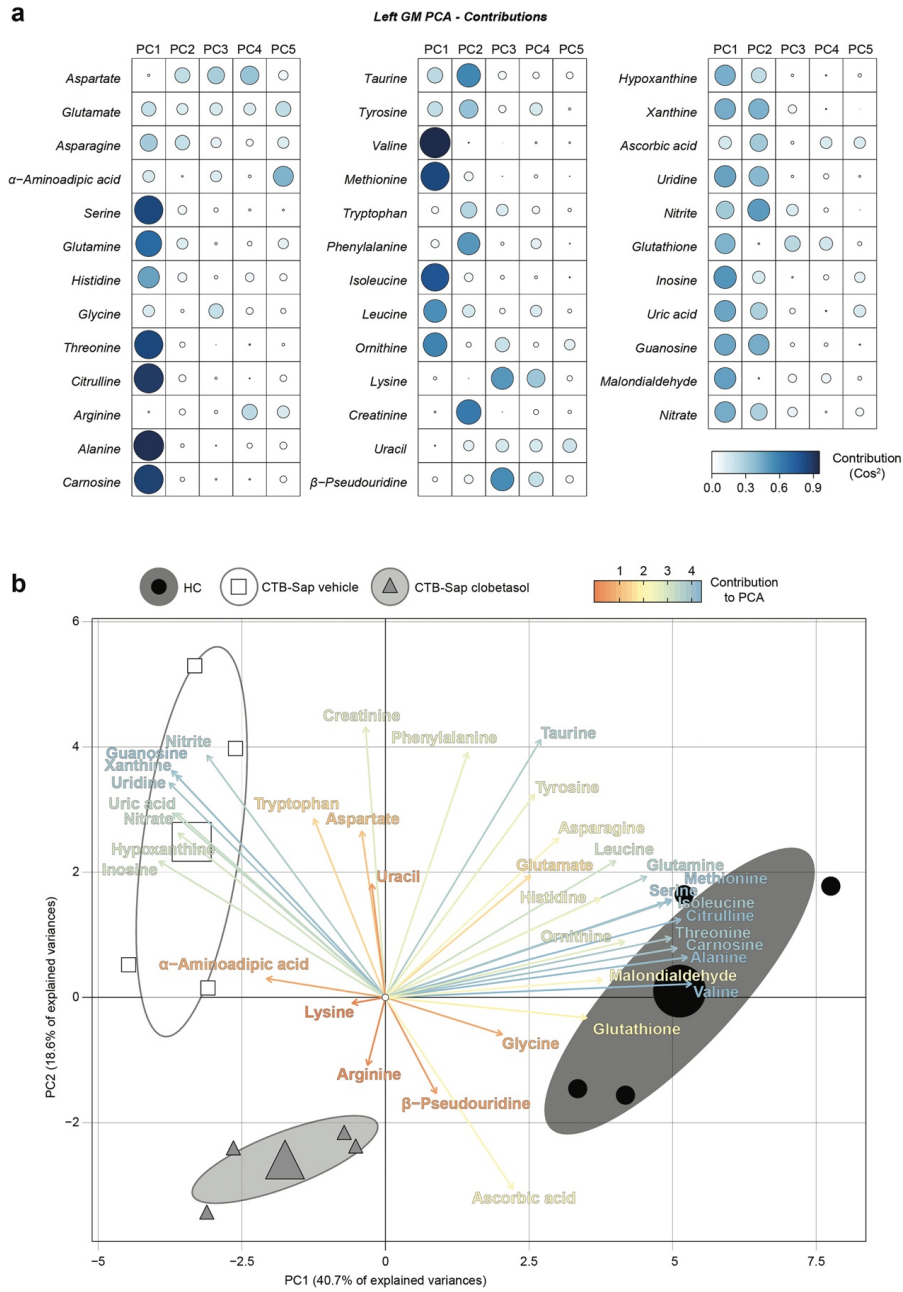


**Fig. S6. Principal components analysis (PCA) of left GM metabolites of HC, CTB-Sap vehicle and CTB-Sap clobetasol mice. a.** Factor map of quality plot representation of the variables on PC1-PC5 expressed as cosine squared (Cos<sup>2</sup>). **b.** PCA biplot of 37 metabolites for HC,

CTB-Sap vehicle and CTB-Sap clobetasol; key-colored arrows represent the contribution of each variable to the PCA; small circles/squares/triangles represent single subjects and large circles/squares/triangles represents the mean point of the confidence ellipses.



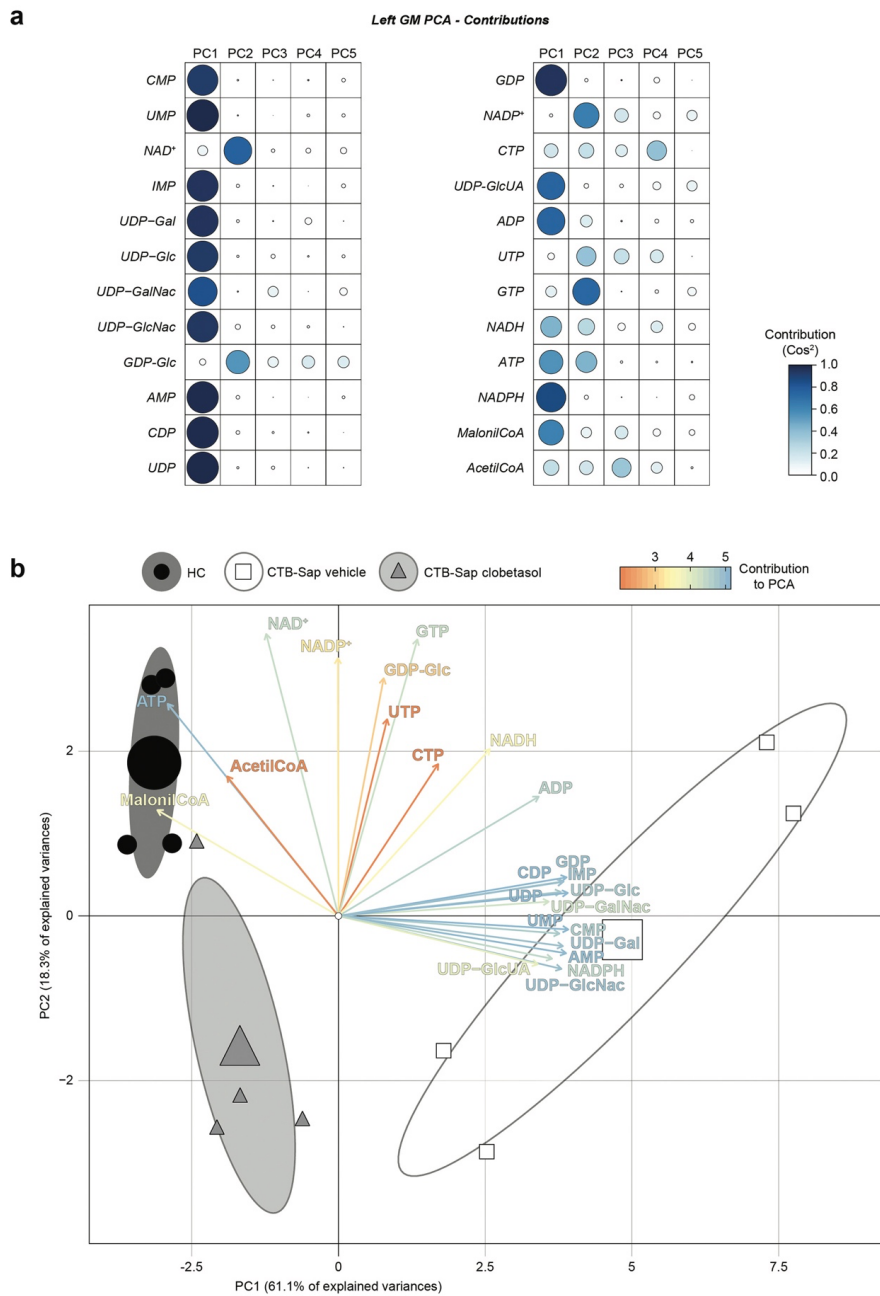


**Fig. S7. Principal components analysis (PCA) of left GMS metabolites of HC, CTB-Sap vehicle and CTB-Sap clobetasol mice.** **a**, Factor map of quality plot representation of the variables on PC1-PC5 expressed as square cosine (Cos<sup>2</sup>). **b**, PCA biplot of 24 metabolites for HC,

CTB-Sap vehicle and CTB-Sap clobetasol; key-colored arrows represent the contribution of each variable to the PCA; small circles/squares/triangles represent single subjects and large circles/squares/triangles represents the mean point of the confidence ellipses.

## **CONCLUDING REMARKS**

Non autonomous cells have a key role in exacerbating the neurotoxic milieu that leads to MNs death and then to paralysis in ALS, as a final result (Van Harten, Phatnani et al. 2021). Among these, glial cells (i.e. astrocytes and microglia), which physiologically ensure and maintain homeostatic conditions within the central nervous system, consequentially influencing also neuronal activity, are demonstrated to be involved in sustaining neuroinflammation and neurotoxicity in several neurological disorders (Van Harten, Phatnani et al. 2021) (Clarke and Patani 2020) (Glass, Saijo et al. 2010).

To better clarify the neuro-glial crosstalk in human ALS and in an experimental model of selective motoneuronal depletion (CTB-Sap model), we investigated the expression of the main hemichannel-forming astroglial connexin involved in cell-to cell communication, which is connexin 43 (Cx43) (Vicario, Zappala et al. 2017) (Vicario and Parenti 2022). Particularly, in human sporadic ALS transcriptome of central nervous system dataset we found reactive astrogliosis and Cx43 upregulation positively correlated each other. We then moved to assess Cx43 signal in CTB-Sap model. A first characterization of the model demonstrated to be able to induce a depletion of about 50% of MNs, which is reflected in impaired locomotion and findings of typical electromyographic denervation signs similar to ALS patients (i.e. fibrillations, positive sharps waves and fasciculations) (de Carvalho, Dengler et al. 2008), suggesting that such model may be useful to reproduce and study motoneuronal loss effects for neurodegenerative diseases and ALS. Pathophysiological analysis of the resident glial cell population in motoneuron depleted spinal cord revealed astrogliosis, coupled with Cx43 increased levels, sign of increased astrocyte-astrocyte and astrocytes-microglia communication, which also entails the exchange of toxic molecules and metabolites. These results suggest the hypothesis that glial population among spared MNs responds to the lesion increasing Cx43-based cell-to cell communication, which may contribute to generate a toxic circuit affecting neuronal survival.

We then moved to study the Shh signaling pathway, for its role in sustaining/supporting neuroplasticity and for its known disruption in neurodegenerative diseases as mentioned before.

We verified the involvement of Shh signaling pathway in ALS patients' transcriptomes and we found that there was an overall downregulation of the pathway, with a significant reduction of players of the pathway, such the Shh receptor Patch and the nuclear effector Gli1, but without observing significant variations of the coreceptor Smo, suggesting that if

Smo remains unchanged, it may be considered among druggable targets for ALS and for neuronal loss diseases in general. Such phenomenon prompted us to evaluate Shh pathway in our motoneuron depleted CTB-Sap model, and its potential modulation using clobetasol, which activates the canonical Shh pathway acting as a Smo agonist. Next, clobetasol effects were analyzed by functional, pathophysiological, and metabolic point of view. Thus, we treated CTB-Sap lesioned mice weekly with clobetasol, starting from 7 days post lesion (dpl), when mice showed a peak of impaired motor symptoms, up to 42 dpl, when lesion effects are still behaviorally stable and visible. What we found was that clobetasol was able to revert such motor impairment as early as the first week post treatment and the improvement persisted till the end of the experimental time. This functional recovery was coupled with reduced electromyographic signs of muscle denervation and recovered cholinergic transmission at neuromuscular junction level, suggesting that clobetasol is able to ameliorate behavioral impairment promoting muscle reinnervation.

As the proportion of depleted MNs did not change, confirming the efficacy of the neurotoxic lesion in both CTB-Sap and CTB-Sap-clobetasol treated mice, we moved to the study of the spinal pathophysiology to link such phenomenon to possible plastic and compensatory changes among spared MNs in the site of the lesion.

We first found that the overall downregulation of Shh pathway in spinal resident population after CTB-Sap lesion, detected as a reduced nuclear Gli1 translocation, with a significant reduction in astrocytes, was reverted by clobetasol, which increased nuclear Gli1 in both neurons and astrocytes; we also noticed that clobetasol promoted newly form synapses among spared MNs, that collectively indicates that clobetasol supports the onset of spinal cord plasticity through Shh pathway upregulation.

Moreover, the analysis of spinal metabolites in CTB-Sap and CTB-Sap-clobetasol treated groups, showed mainly a significant modulation of metabolites involved in glycolysis and tricarboxylic acid cycle (i.e. lysine, tryptophan, isoleucine and arginine) and a significant reversion to near normal levels of hypoxanthine and xanthine following clobetasol treatment. Of note, we noticed that motoneuronal loss induced downregulation of inhibitory neurotransmitters, such as GABA and glycine, whereas the excitatory glutamate-based neurotransmission did not change as compared to healthy control group, meaning that a same quantity of glutamate, acting on a reduced proportion of MNs in CTB-Sap lesioned mice, in this manner leads to overstimulation and then to excitotoxic effects, those also amplified by impaired inhibitory GABA and glycine circuitries; in this context, clobetasol

treatment was found to increase both GABA and glycine levels, thus promoting a rebalance of neuronal transmission.

Furthermore, we moved to characterize the phenotype of spinal immune cells resident in the spinal cord, and what we found was that in CTB-Sap lesioned spinal cord, motoneuronal loss induced reactive astrocytes among the neighboring MNs left, with a concomitant increase of polarized microglia (CD206<sup>+</sup> and CD80<sup>+</sup>), highlighting a pro-inflammatory response. In this context, clobetasol treatment showed immunomodulatory and anti-inflammatory effects, reverting astrocytes phenotype and microglia polarization, but also inducing an overall downregulation of B and T NK lymphocytes.

We then assessed the impact of motoneuronal loss on muscle. The study of muscular physiopathology revealed atrophy, reduced fiber dimension and increased percentage of centrally located nuclei, this last indicating an attempt of the muscle to regenerate upon lesion. Clobetasol, instead, enhanced muscle repair and regenerative mechanisms reestablishing muscular morphology and microenvironment, as confirmed by increased muscle fiber dimension, increased Pax7<sup>+</sup> cells (indicating proliferative events), together with a significant increase of the proportion of anti-inflammatory infiltrating macrophages (F4/80 and Arg1 double positive) into denervated and clobetasol treated muscle.

We then focused on the characterization of the metabolic profile of the muscle to find some evidence about muscle energy state and wellness. We mainly found that denervation affected muscle metabolism, leading to a significant accumulation of IMP, hypoxanthine and xanthine, and uric acid, with a concomitant downregulation of malonil-CoA levels, which collectively indicate an alteration of purine metabolism, which concurs to amplify the unfavorable microenvironment by the production of reactive oxygen species, and a disrupt of fatty acid metabolism. This condition was reverted by clobetasol promoting a metabolic shift. Moreover, metabolic imbalance of CTB-Sap muscle was also confirmed by the alteration of both mitochondrial morphology and function, as we found that denervation induced mitochondrial fission and also accumulation of energetic substrates monophosphates, at the expense of triphosphates with a reduction of ATP, coupled with accumulation of glycosylated UDP-derivates and predominance of a reduced mitochondrial redox potential. Such effects were once again reverted by clobetasol treatment, which restored mitochondrial fitness and metabolism. Taken all these findings together, we claim that clobetasol has multi-system effects acting simultaneously in spinal cord and cell muscle, and through the canonical Shh signaling pathway activation, the immunomodulation, and the metabolic rebalancing, leads to neuromuscular plasticity and compensatory

mechanisms that together facilitate functional recovery upon motoneuronal loss-induced motor impairment. For all these reasons, considering also that clobetasol is an approved drug, it may be suggested to be used as a repositioning drug for a translational use in denervating and neurodegenerative disease approaches such ALS.

## **REFERENCES (INTRODUCTION AND CONCLUDING REMARKS)**

- Belgacem, Y. H., A. M. Hamilton, S. Shim, K. A. Spencer and L. N. Borodinsky (2016). "The Many Hats of Sonic Hedgehog Signaling in Nervous System Development and Disease." J Dev Biol **4**(4).
- Bhandari, R., A. Kuhad and A. Kuhad (2018). "Edaravone: a new hope for deadly amyotrophic lateral sclerosis." Drugs Today (Barc) **54**(6): 349-360.
- Bolshakov, A. P., M. Y. Stepanichev, Y. V. Dobryakova, Y. S. Spivak and V. A. Markevich (2020). "Saporin from *Saponaria officinalis* as a Tool for Experimental Research, Modeling, and Therapy in Neuroscience." Toxins (Basel) **12**(9).
- Brooks, B. R. (1994). "El Escorial World Federation of Neurology criteria for the diagnosis of amyotrophic lateral sclerosis. Subcommittee on Motor Neuron Diseases/Amyotrophic Lateral Sclerosis of the World Federation of Neurology Research Group on Neuromuscular Diseases and the El Escorial "Clinical limits of amyotrophic lateral sclerosis" workshop contributors." J Neurol Sci **124 Suppl**: 96-107.
- Brown, R. H. and A. Al-Chalabi (2017). "Amyotrophic Lateral Sclerosis." N Engl J Med **377**(2): 162-172.
- Caller, T. A., J. W. Doolin, J. F. Haney, A. J. Murby, K. G. West, H. E. Farrar, A. Ball, B. T. Harris and E. W. Stommel (2009). "A cluster of amyotrophic lateral sclerosis in New Hampshire: a possible role for toxic cyanobacteria blooms." Amyotroph Lateral Scler **10 Suppl 2**: 101-108.
- Campanari, M. L., M. S. Garcia-Ayllon, S. Ciura, J. Saez-Valero and E. Kabashi (2016). "Neuromuscular Junction Impairment in Amyotrophic Lateral Sclerosis: Reassessing the Role of Acetylcholinesterase." Front Mol Neurosci **9**: 160.
- Clarke, B. E. and R. Patani (2020). "The microglial component of amyotrophic lateral sclerosis." Brain **143**(12): 3526-3539.
- Cox, P. A., S. A. Banack and S. J. Murch (2003). "Biomagnification of cyanobacterial neurotoxins and neurodegenerative disease among the Chamorro people of Guam." Proc Natl Acad Sci U S A **100**(23): 13380-13383.
- de Carvalho, M., R. Dengler, A. Eisen, J. D. England, R. Kaji, J. Kimura, K. Mills, H. Mitsumoto, H. Nodera, J. Shefner and M. Swash (2008). "Electrodiagnostic criteria for diagnosis of ALS." Clin Neurophysiol **119**(3): 497-503.

Drannik, A., J. Martin, R. Peterson, X. Ma, F. Jiang and J. Turnbull (2017). "Cerebrospinal fluid from patients with amyotrophic lateral sclerosis inhibits sonic hedgehog function." PLoS One **12**(2): e0171668.

Fischer, L. R., D. G. Culver, P. Tennant, A. A. Davis, M. Wang, A. Castellano-Sanchez, J. Khan, M. A. Polak and J. D. Glass (2004). "Amyotrophic lateral sclerosis is a distal axonopathy: evidence in mice and man." Exp Neurol **185**(2): 232-240.

Garcia-Garcia, R., L. Martin-Herrero, L. Blanca-Pariente, J. Perez-Cabello and C. Roodveldt (2021). "Immune Signaling Kinases in Amyotrophic Lateral Sclerosis (ALS) and Frontotemporal Dementia (FTD)." Int J Mol Sci **22**(24).

Glass, C. K., K. Saijo, B. Winner, M. C. Marchetto and F. H. Gage (2010). "Mechanisms underlying inflammation in neurodegeneration." Cell **140**(6): 918-934.

Gois, A. M., D. M. F. Mendonca, M. A. M. Freire and J. R. Santos (2020). "In Vitro and in Vivo Models of Amyotrophic Lateral Sclerosis: An Updated Overview." Brain Res Bull **159**: 32-43.

Goutman, S. A., O. Hardiman, A. Al-Chalabi, A. Chio, M. G. Savelieff, M. C. Kiernan and E. L. Feldman (2022). "Emerging insights into the complex genetics and pathophysiology of amyotrophic lateral sclerosis." Lancet Neurol **21**(5): 465-479.

Goutman, S. A., O. Hardiman, A. Al-Chalabi, A. Chio, M. G. Savelieff, M. C. Kiernan and E. L. Feldman (2022). "Recent advances in the diagnosis and prognosis of amyotrophic lateral sclerosis." Lancet Neurol **21**(5): 480-493.

Gulino, R., N. Vicario, M. A. S. Giunta, G. Spoto, G. Calabrese, M. Vecchio, M. Gulisano, G. Leanza and R. Parenti (2019). "Neuromuscular Plasticity in a Mouse Neurotoxic Model of Spinal Motoneuronal Loss." Int J Mol Sci **20**(6).

Hardiman, O., A. Al-Chalabi, A. Chio, E. M. Corr, G. Logroscino, W. Robberecht, P. J. Shaw, Z. Simmons and L. H. van den Berg (2017). "Amyotrophic lateral sclerosis." Nat Rev Dis Primers **3**: 17071.

Johnsen, B. (2020). "Diagnostic criteria for amyotrophic lateral sclerosis from El Escorial to Gold Coast." Clin Neurophysiol **131**(8): 1962-1963.

Le Gall, L., E. Anakor, O. Connolly, U. G. Vijayakumar, W. J. Duddy and S. Duguez (2020). "Molecular and Cellular Mechanisms Affected in ALS." J Pers Med **10**(3).

Llewellyn-Smith, I. J., C. L. Martin, L. F. Arnolda and J. B. Minson (2000). "Tracer-toxins: cholera toxin B-saporin as a model." J Neurosci Methods **103**(1): 83-90.

Mejzini, R., L. L. Flynn, I. L. Pitout, S. Fletcher, S. D. Wilton and P. A. Akkari (2019). "ALS Genetics, Mechanisms, and Therapeutics: Where Are We Now?" Front Neurosci **13**: 1310.

Moloney, E. B., F. de Winter and J. Verhaagen (2014). "ALS as a distal axonopathy: molecular mechanisms affecting neuromuscular junction stability in the presymptomatic stages of the disease." Front Neurosci **8**: 252.

Murch, S. J., P. A. Cox, S. A. Banack, J. C. Steele and O. W. Sacks (2004). "Occurrence of beta-methylamino-L-alanine (BMAA) in ALS/PDC patients from Guam." Acta Neurol Scand **110**(4): 267-269.

Najm, F. J., M. Madhavan, A. Zaremba, E. Shick, R. T. Karl, D. C. Factor, T. E. Miller, Z. S. Nevin, C. Kantor, A. Sargent, K. L. Quick, D. M. Schlatzer, H. Tang, R. Papoian, K. R. Brimacombe, M. Shen, M. B. Boxer, A. Jadhav, A. P. Robinson, J. R. Podojil, S. D. Miller, R. H. Miller and P. J. Tesar (2015). "Drug-based modulation of endogenous stem cells promotes functional remyelination in vivo." Nature **522**(7555): 216-220.

Oskarsson, B., T. F. Gendron and N. P. Staff (2018). "Amyotrophic Lateral Sclerosis: An Update for 2018." Mayo Clin Proc **93**(11): 1617-1628.

Ramroop, H. and R. Cruz (2022). Electrodiagnostic Evaluation Of Motor Neuron Disease. StatPearls. Treasure Island (FL).

Shefner, J. M., A. Al-Chalabi, M. R. Baker, L. Y. Cui, M. de Carvalho, A. Eisen, J. Grosskreutz, O. Hardiman, R. Henderson, J. M. Matamala, H. Mitsumoto, W. Paulus, N. Simon, M. Swash, K. Talbot, M. R. Turner, Y. Ugawa, L. H. van den Berg, R. Verdugo, S. Vucic, R. Kaji, D. Burke and M. C. Kiernan (2020). "A proposal for new diagnostic criteria for ALS." Clin Neurophysiol **131**(8): 1975-1978.

Talbott, E. O., A. M. Malek and D. Lacomis (2016). "The epidemiology of amyotrophic lateral sclerosis." Handb Clin Neurol **138**: 225-238.

Traiffort, E., E. Angot and M. Ruat (2010). "Sonic Hedgehog signaling in the mammalian brain." J Neurochem **113**(3): 576-590.

Ugbode, C. I., I. Smith, B. J. Whalley, W. D. Hirst and M. Rattray (2017). "Sonic hedgehog signalling mediates astrocyte crosstalk with neurons to confer neuroprotection." J Neurochem **142**(3): 429-443.

Van Harten, A. C. M., H. Phatnani and S. Przedborski (2021). "Non-cell-autonomous pathogenic mechanisms in amyotrophic lateral sclerosis." Trends Neurosci **44**(8): 658-668.

Verma, S., S. Khurana, A. Vats, B. Sahu, N. K. Ganguly, P. Chakraborti, M. Gourie-Devi and V. Taneja (2022). "Neuromuscular Junction Dysfunction in Amyotrophic Lateral Sclerosis." Mol Neurobiol **59**(3): 1502-1527.

Vicario, N., J. D. Bernstock, F. M. Spitale, C. Giallongo, M. A. S. Giunta, G. Li Volti, M. Gulisano, G. Leanza, D. Tibullo, R. Parenti and R. Gulino (2019). "Clobetasol Modulates



Adult Neural Stem Cell Growth via Canonical Hedgehog Pathway Activation." Int J Mol Sci **20**(8).

Vicario, N. and R. Parenti (2022). "Connexins Signatures of the Neurovascular Unit and Their Physio-Pathological Functions." Int J Mol Sci **23**(17).

Vicario, N., A. Zappala, G. Calabrese, R. Gulino, C. Parenti, M. Gulisano and R. Parenti (2017). "Connexins in the Central Nervous System: Physiological Traits and Neuroprotective Targets." Front Physiol **8**: 1060.

Xu, L., T. Liu, L. Liu, X. Yao, L. Chen, D. Fan, S. Zhan and S. Wang (2020). "Global variation in prevalence and incidence of amyotrophic lateral sclerosis: a systematic review and meta-analysis." J Neurol **267**(4): 944-953.

Yamanaka, K. and O. Komine (2018). "The multi-dimensional roles of astrocytes in ALS." Neurosci Res **126**: 31-38.

Yang, C., Y. Qi and Z. Sun (2021). "The Role of Sonic Hedgehog Pathway in the Development of the Central Nervous System and Aging-Related Neurodegenerative Diseases." Front Mol Biosci **8**: 711710.

## PAPERS

**Spitale FM**, Vicario N, Rosa MD, Tibullo D, Vecchio M, Gulino R, Parenti R. Increased expression of connexin 43 in a mouse model of spinal motoneuronal loss. *Aging (Albany NY)*. 2020 Jun 24;12(13):12598-12608. doi: 10.18632/aging.103561. Epub 2020 Jun 24. PMID: 32579130; PMCID: PMC7377853.

Vicario N, **Spitale FM**, Tibullo D, Giallongo C, Amorini AM, Scandura G, Spoto G, Saab MW, D'Aprile S, Alberghina C, Mangione R, Bernstock JD, Botta C, Gulisano M, Buratti E, Leanza G, Zorec R, Vecchio M, Di Rosa M, Li Volti G, Lazzarino G, Parenti R, Gulino R. Clobetasol promotes neuromuscular plasticity in mice after motoneuronal loss via sonic hedgehog signaling, immunomodulation and metabolic rebalancing. *Cell Death Dis*. 2021 Jun 16;12(7):625. doi: 10.1038/s41419-021-03907-1. PMID: 34135312; PMCID: PMC8209072.

## Others

Vicario N, Turnaturi R, **Spitale FM**, Torrisi F, Zappalà A, Gulino R, Pasquinucci L, Chiechio S, Parenti C, Parenti R. Intercellular communication and ion channels in neuropathic pain chronicization. *Inflamm Res*. 2020 Sep;69(9):841-850. doi: 10.1007/s00011-020-01363-9. Epub 2020 Jun 12. PMID: 32533221.

Torrisi F, Vicario N, **Spitale FM**, Cammarata FP, Minafra L, Salvatorelli L, Russo G, Cuttone G, Valable S, Gulino R, Magro G, Parenti R. The Role of Hypoxia and SRC Tyrosine Kinase in Glioblastoma Invasiveness and Radioresistance. *Cancers (Basel)*. 2020 Oct 4;12(10):2860. doi: 10.3390/cancers12102860. PMID: 33020459; PMCID: PMC7599682.

Fidilio A, Grasso M, Turnaturi R, Caruso G, **Spitale FM**, Vicario N, Parenti R, Spoto S, Musso N, Marrazzo A, Chiechio S, Caraci F, Pasquinucci L, Parenti C. The Multimodal MOPr/DOPr Agonist LP2 Reduces Allodynia in Chronic Constriction Injured Rats by Rescue of TGF- $\beta$ 1 Signalling. *Front Pharmacol*. 2021 Oct 6;12:749365. doi: 10.3389/fphar.2021.749365. PMID: 34690781; PMCID: PMC8526862.

Vicario N, Denaro S, Turnaturi R, Longhitano L, **Spitale FM**, Spoto S, Marrazzo A, Zappalà A, Tibullo D, Li Volti G, Chiechio S, Pasquinucci L, Parenti R, Parenti C. *Mu and Delta Opioid Receptor Targeting Reduces Connexin 43-Based Heterocellular Coupling during Neuropathic Pain. Int J Mol Sci. 2022 May 24;23(11):5864. doi: 10.3390/ijms23115864. PMID: 35682543; PMCID: PMC9180638.*

## **ACKNOWLEDGEMENTS**

I would like to thank everyone who has supported me during these years.

First, I would like to thank Professor Parenti, Professor Vicario and Professor Li Volti for their careful supervision, courtesy and willingness.

They gave me the chance to touch by hand what the research is and what is meant for a real research team. They taught me the importance to be a solid group and how much important the contribute of every component is. Particularly, I have to thank Professor Parenti for her advice about work and life, and for her sweet personality. Likewise, I have to thank Professor Vicario, who besides being a constant guidance and point of reference, also helped me to grow my self-esteem and build my knowledge. Thanks also to Professor Li Volti who supervised me, for his professionalism and wisdom.

I would also thank the PhD coordinator Professor Bucolo, for his kindness and precise indications during the course.

I have also to thanks all my past and present lab members, in particular Grazia, Simona D.A., Cristiana, Filippo, Anna, Simona D. and Carla, who supported me both physically and psychologically, contributing to make the place of work as a second family.

Thanks also to Professor Sanchez Martín, who gave me the opportunity to work in her laboratory in Granada, with the fundamental guidance of Victoria. Thanks to all the Spanish team research and my new friends Mónica, Federica, Rocío, Isa, Paula y Ana.

Without any doubt, I have to thank the most my family, for all the patience and all the love they give me every day. Thanks to my mother, who has always believed in myself. We have repeated daily: “everything will be fine”, and it was.

Thanks to my best friends Aurora, Lucrezia, Emanuela and Claudia to be light in moments of darkness. Thanks to Diego, for bringing me love, happiness and new future.